SANDIA REPORT
SAND2008-7710
Unlimited Release
Printed November 2008

Toxicological studies of semiconductor quantum dots on immune cells

Marlene Bachand, Amanda Carroll-Portillo, Adrienne C. Greene, Lynette Rios, J. Bryce Ricken, Jens Poschet, and George D. Bachand

Prepared by
Sandia National Laboratories
Albuquerque, New Mexico 87185 and Livermore, California 94550

Sandia is a multiprogram laboratory operated by Sandia Corporation,
a Lockheed Martin Company, for the United States Department of Energy's
National Nuclear Security Administration under Contract DE-AC04-94AL85000.

Issued by Sandia National Laboratories, operated for the United States Department of Energy by Sandia Corporation.

Available to DOE and DOE contractors from
U.S. Department of Energy
Office of Scientific and Technical Information
P.O. Box 62
Oak Ridge, TN 37831

Telephone: (865) 576-8401
Facsimile: (865) 576-5728
E-Mail: reports@adonis.osti.gov
Online ordering: http://www.osti.gov/bridge

Available to the public from
U.S. Department of Commerce
National Technical Information Service
5285 Port Royal Rd.
Springfield, VA 22161

Telephone: (800) 553-6847
Facsimile: (703) 605-6900
E-Mail: orders@ntis.fedworld.gov
Online order: http://www.ntis.gov/help/ordermethods.asp?loc=7-4-0#online

SAND2008-7710
Unlimited Release
Printed November 2008

Toxicological studies of semiconductor quantum dots on immune cells

Marlene Bachand,[1] Amanda Carroll-Portillo,[1] Adrienne C. Greene,[1] Lynette Rios,[1] J. Bryce Ricken,[2] Jens Poschet,[2] and George D. Bachand[1]

[1] CINT Science, Physical, Chemical, and Nanosciences Center
[2] Biomolecular Analysis and Imaging, Biological and Energy Sciences Center

Sandia National Laboratories
P.O. Box 5800, MS1303
Albuquerque, NM 87185-1303

Abstract

Nanoengineered materials hold a vast promise of enabling revolutionary technologies, but also pose an emerging and potentially serious threat to human and environmental health. While there is increasing knowledge concerning the risks posed by engineered nanomaterials, significant inconsistencies exist within the current data based on the high degree of variability in the materials (e.g., synthesis method, coatings, etc) and biological test systems (e.g., cell lines, whole organism, etc). In this project, we evaluated the uptake and response of two immune cell lines (RAW macrophage and RBL mast cells) to nanocrystal quantum dots (Qdots) with different sizes and surface chemistries, and at different concentrations. The basic experimental design followed a 2 x 2 x 3 factorial model: two Qdot sizes (Qdot 520 and 620), two surface chemistries (amine "NH_2" and carboxylic acid "COOH"), and three concentrations (0, 1 nM, and 1 μM). Based on this design, the following Qdots from Evident Technologies were used for all experiments: Qdot 520-COOH, Qdot 520-NH_2, Qdot 620-COOH, and Qdot 620-NH_2. Fluorescence and confocal imaging demonstrated that Qdot 620-COOH and Qdot 620-NH_2 nanoparticles had a greater level of internalization and cell membrane association in RAW and RBL cells, respectively. From these data, a two-way interaction between Qdot size and concentration was observed in relation to the level of cellular uptake in RAW cells, and association with RBL cell membranes. Toxicity of both RBL and RAW cells was also significantly dependent on the interaction of Qdot size and concentration; the 1 μM concentrations of the larger, Qdot 620 nanoparticles induced a greater toxic effect on both cell lines. The RBL data also demonstrate that Qdot exposure can induce significant toxicity independent of cellular uptake. A significant increase in TNF-α and decrease in IL-10 release was observed in RAW cells, and suggested that Qdot exposure induced a pro-inflammatory response. In contrast, significant decreases in both TNF-α and IL-4 releases were observed in RBL cells, which is indicative of a suppressed inflammatory response. The changes in cytokine release observed in

RAW and RBL cells were primarily dependent on Qdot concentration and independent of size and surface chemistry. Changes in the activity of superoxide dismutase were observed in RAW, but not RBL cells, suggesting that RAW cells were experiencing oxidative stress induced by Qdot exposure. Overall, our results demonstrate that the uptake/association and biomolecular response of macrophage and mast cells is primarily driven by an interaction between Qdot size and concentration. Based on these findings, a more detailed understanding of how size directly impacts cellular interactions and response will be critical to developing predictive models of Qdot toxicity

Acknowledgments

This work was supported by Sandia's Laboratory Directed Research and Development (LDRD) Project 128712. Sandia is a multiprogram laboratory operated by Sandia Corporation, a Lockheed Martin Company, for the United States Department of Energy under Contract DE-AC04-94AL85000.

Table of Contents

List of Tables

List of Figures

1.0 Introduction

Nanotechnology holds a vast promise of enabling a wide range of transformational technologies such as enhanced photovoltaics,[1-3] novel biomedical imaging tools,[4-6] and targeted drug delivery and therapeutics.[7-9] The rapid development of nanotechnology, however, has recently faced challenges due to potential risks with respect to human and the environmental health.[10-15] The National Nanotechnology Initiative defines nanoscience as "research to discover new behaviors and properties of materials with dimensions at the nanoscale which ranges roughly from 1 to 100 nanometers (nm)." A key aspect to this definition involves the new behaviors and properties that exist only at the nanoscale. While these properties and behaviors may be used to achieve significant gains (e.g., highly efficient energy transfer), they also raise important and unique concerns with regard to human health impact and environmental contamination by such materials. Currently, the health impacts associated with nanoengineered materials are poorly understood.[16] Reports such as the ability of carbon nanotubes to cross the blood-brain barrier, however, suggest that the risks are real and potentially serious.[17,18] More recently, asbestos-like pathogenicity has been observed in mice exposed to carbon nanotubes,[19,20] increasing fears over the serious risks associated with engineering nanomaterials. The environmental health and safety issues facing nanoscience and nanotechnology are strikingly similar to those faced during the rise of biotechnology, in which initial excitement and promise were met with increasing public scrutiny and fear.[21-26] Thus, there is a critical need at the global level to develop a fundamental understanding of the acute and chronic toxicological effects of engineered nanomaterials before fear and misconceptions impede future development.

The synthesis, characterization, and application of nanoparticles and nanotubes derived from carbon-based,[27-30] metallic,[31-35] and semiconductor[36-40] materials have been widely reported in the literature. In particular, quantum dots (Qdots) have been extensively studied as fluorescent reporters for biomedical imaging.[6,8,36,41] Qdots are composite nanocrystals composed of a semiconductor core (e.g., group II-VI and IV-VI materials), a ZnS shell, and often a polymer coating that enables water solubility and biological application (Figure 1).[42,43] The luminescent properties of QDots depend directly of the size of the core, which can be precisely controlled during synthesis and produce Qdots with emission spectra across the visible range and into the infrared range.[31,38,41] Molecular dyes are being increasingly replaced by Qdots for *in vitro* biological imaging based on the enhanced photostability and broad excitation and size-dependent emission spectra of Qdots.[7,41] *In vivo* applications of Qdots have been rather limited, however, as the toxicity of Qdots has not been fully characterized. In addition, the documented acute and chronic toxicity of the core materials such as cadmium (Cd) and lead (Pb)[44] has increased the environmental health and safety awareness of Qdots in laboratory applications.

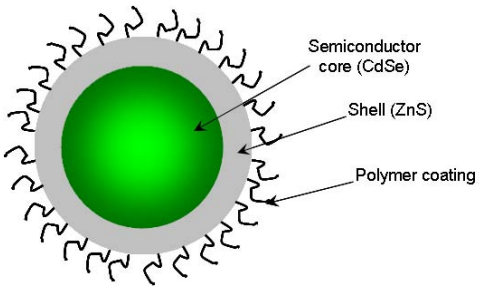

Figure 1. Anatomy of a quantum dot (Qdot). The central core is composed of a semiconductor material such as CdSe, which is encapsulated with a ZnS shell. The Qdot is then coated with a polymer to enable water solubility.

The toxicology of CdSe Qdots has been investigated in mouse model systems and a variety of cultured mammalian cells. These studies demonstrate a wide range in effects, from no abnormal behaviors/effects to high levels of toxicity and DNA damage.[16] The broad spectrum of results is due to a number of factors including varied surface coatings, exposure conditions, and Qdot concentration. The ability to synthesize Qdots with a diverse set of physical properties (e.g., size, shape, composition, surface chemistry, etc.) creates an immense, multidimensional problem in assessing toxicological effects, and a critical challenge for predictive risk assessment. The primary goal of this project was to establish fundamental relationships between the physical and chemical properties of engineered nanoparticles and the associated biomolecular interactions and response of cells. Here we demonstrate that the interaction, uptake, and response of macrophage and mast cells are strongly dependent on the interaction between Qdot size and concentration.

2.0 Materials & Methods

2.1 Cell lines and Qdots

Two specific cell types were used for these studies: RAW 264.7 (mouse leukemic macrophage cell line) and RBL-2H3 (rat basophilic leukemia mast cells). Macrophages are the "professional phagocytes" responsible for removing unwanted biotic and abiotic materials, and initiating/propagating inflammatory reactions and oxidative stress. Mast cells also play an important role in inflammatory processes, particularly allergic reactions, through the rapid release of granules and hormonal mediators. RAW cells were maintained at 37º C with 5% CO_2 in DMEM10 (Dulbecco's Modified Eagle Medium media containing 10% fetal bovine serum; Hyclone, Logan, UT) and 1% penicillin-streptomycin. Cells were seeded in a glass-bottom 96-well plate at a density of 10^5 per well. RBL cells were maintained at 37º C with 5% CO_2, in MEM15 (Minimum Essential Media containing 15% fetal bovine serum; Hyclone, Logan, UT) and 1% penicillin-streptomycin. Cells were seeded in a glass-bottom 96-well plate at a density of 10^5 per well.

Commercially available semiconductor nanocrystal QDots (Evident Technologies, Troy, NY) were used as the model system based on their ubiquitous use in the research field. The cadmium and selenium used for synthesis of the cores of these particles raises important issues regarding the toxicological effects in humans. Qdots of two different sizes/emission peaks (Qdot 520: EviFluor™ 520; Qdot 620: EviFluor™ 620) and surface chemistries (amine, -NH_2 and carboxylic acid, -COOH groups) were investigated. Safety information (e.g., MSDS toxicology information) for these Qdots is currently not available, aside from inferences based on the bulk metals. Three concentrations of the Qdots were tested: 0 (negative control), 1 nM, and 1 µM. The photoluminescence of the different Qdots was characterized by fluorimetry in the different media (i.e., water, DMEM10, and MEM15) to evaluate potential changes in spectra properties. Fluorescence was measured in each solution for the different Qdots sizes, surface functionalities, and concentrations. Integration of the intensity curves was determined using Spectra Solve software (Ames Photonics, Inc., Hurst, Texas). The values were measured by integrating the area under the curve of the same band pass values as used for taking the epifluorescence images.

2.2 Experimental design and analysis

RBL and RAW cells were seeded into glass-bottom 96-well plate at a density of 10^5 per well, and allowed to adhere for 4 hours. Qdots (Qdot 520-NH_2 and -COOH; Qdot 620-NH_2 and -COOH) were then added to each well to give final concentrations of either 1 nM or 1µM. An equal volume of water was added to negative control wells. All treatments were repeated in triplicates on a given plate; the entire experiment was repeated to ensure quality control. Qdots were maintained in the culture medium for 18 hours. After this period, the plates were centrifuged in a swinging bucket rotor at 400 *x g* for 4 min. Cells were then washed gently with a phosphate buffer saline solution (PBS) lacking magnesium and calcium, and centrifuged at 400 *x g* for 4 min. Once the appropriate media was replaced, brightfield and fluorescence imaging was then performed as detailed below. At 42 hours post-Qdot exposure, the cells were treated and imaged by brightfield and fluorescence microscopy as described for the 18 hour incubation.

The experiments were executed to give a 2 x 2 x 3 factorial design with the following parameters: size (Qdot 520 and Qdot 620), surface chemistry (NH_2 and COOH), and concentration (0, 1 nM, and 1 µM). Significant main effects and interactions were analyzed by Three-Way Analysis of Variance, and the Holm-Sidak method for pair wise comparisons.

2.3 Fluorescence microscopy and analysis

Fluorescence and brightfield microscopy were used to evaluate Qdot uptake and cell viability at 18 and 42 hours post-Qdot exposure. All imaging was performed on an Olympus IX-71 inverted microscope with a 60× oil immersion lens. Fluorescence and brightfield still images were collected using a Hamamatsu Orca or Orca II-ER CCD camera, and subsequently combined and analyzed using MicroSuite AnalySIS software (Olympus Soft Imaging Solution GmbH). The relative fluorescence (RF) of Qdots associated with a cell was estimated by: $RF = I_c/I_b$, where I_c is the mean pixel intensity of the cell, and I_b is the mean pixel intensity of the background. RF values were estimated for 3-5 cells per still image for each of the 12 treatments, three replicates, and duplicate experiments. The confluency of the cells in each image was estimated with five categories: 10 = 0-20%, 30 = 20-40%, 50 = 40-60%, 70 = 60-80%, and 90 = 80-100%. The confluency estimates were averaged across replicates, treatments, and duplicate experiments. The percent of cells with Qdots was estimated by comparing the RF values of the measured cells as compared with the maximum RF value for control cells plus three-times the standard error of the mean.

For confocal microscopy, cells were seeded onto glass coverslips at a density of 10^5 cells. The cells were exposed to the same 1 nM treatments of Qdots as described above. Following 18 hours of exposure, the media was removed and the cells were gently washed with PBS lacking magnesium and calcium. The coverslips were air dried, mounted onto a microscope slide using Cytoseal, and imaged by spinning disk confocal microscopy.

2.4 Inflammatory and oxidative stress response

Biochemical markers associated with inflammatory and oxidative stress pathways were evaluated at 18 hours post-Qdot exposure. RAW 264.7 and RBL-2H3 cells were grown in 6-well plates at a density of 5 x 10^6 cells per well using the previously described culture conditions, and exposed to the various control and Qdot treatments. Following an 18 hour exposure, cells were centrifuged at 400 x g for 4 min in a swinging bucket rotor, and the supernatant was gently removed and stored at -80°C for subsequent cytokine analysis. Cells were then detached by gentle pipetting or cell scraping, and washed with cold PBS. Following centrifugation, the cell pellet was thoroughly resuspended in Cell Lysis Solution (R&D Systems), transferred to a 1.5 mL centrifuge tube, and centrifuged at 14,000 x g for 5 minutes at 4°C. The supernatant was transferred to a clean 1.5 mL centrifuge tube and frozen at -80°C.

Cytokine analysis

The inflammatory response of cells to the different Qdot treatments was characterized by the levels of TNF-α and IL-10, and TNF-α and IL-4 in RAW and RBL cells, respectively. The levels of each cytokine were measured by commercially available enzyme-linked immunosorbent assays (ELISA). For RAW and RBL TNF-α and RAW IL-10 ELISAs (Pierce Biotechnology, EMTNFA, ER3TNFA2, and EM2IL10), 50 µL of cell culture supernatant was loaded onto the plate, and incubated at room temperature for 1 hour for TNF-α assays and 3 hours for the IL-10 assay. Following three sequential washes, a biotinylated anti-TNF-α antibody was added to each well and incubated at room temperature for 1-2 hours. Plates were washed three times, and a streptavidin-HRP conjugate was added and incubated for 30 minutes at room temperature. Following three washes, TMB (3,3´,5,5´-tetramethylbenzidine) was added and incubated at room temperature for 30 minutes, at which time the reaction was stopped with 0.16M sulfuric acid. The absorbance of each well was measured at 450 and 550 nm using a Victor 3 (Perkin Elmer) microplate reader. For the RBL IL-4 ELISA (R&D Systems, R4000) 50 µL of cell culture supernatant was transferred to the ELISA plate and incubated for 2 hours at room temperature, followed by five washes. A solution consisting of horseradish peroxidase-conjugated anti-IL-4 antibodies was then added and incubated for 2 hours at room temperature. After five washes, the TMB substrate was added, incubated for 30 minutes, and stopped with a hydrochloric acid solution. The absorbance of each well was measured at 450 and 550 nm using a Victor 3 (Perkin Elmer) microplate reader. Three-way ANOVA was used to determine significant main effects and interactions.

Superoxide Dismutase activity

The superoxide dismutase activity was measured using a commercially available kit (7500-100-K, R&D Systems), in which the inhibition of nitroblue tetrazolium (NBT)-diformazan formation is used to measure superoxide dismutase activity. The reaction mixture was prepared by mixing 942.5 µL deionized water, 60 µL of 25x Reaction Buffer, 7.5 µL Xanthine solution, 30 µL of NBT solution, and 450 µL of cell lysate that was previously prepared and frozem. After zeroing the spectrophotometer at 550 nm with this solution, 10 µL of xanthine oxidase was added and the absorbance reading was recorded at 30-second intervals for 5 minutes. The rate of increase in absorbance at 550 nm per minute was then calculated for each sample, and used to determine the percent inhibition based on a negative control (i.e., lacking any superoxide dismutase). The superoxide dismutase activity was then estimated based on a standard curve with known levels of the enzyme. Three-way ANOVA was used to determine significant main effects and interactions.

3.0 Results and Discussion

3.1 Spectral analysis of Qdots

Qdots 520 and 620 displayed peak emissions at ~517 nm and ~615 nm, respectively (Figures 1 and 2). The peak emission was not affected by the surface functionality (i.e., -COOH and -NH_2) of the dots, or dilution in the different cell culture media (Figures 2 and 3). However, significant decreases (i.e., quenching) in the fluorescence were observed when the different Qdots were diluted in cell culture media. The integrated fluorescence of each Qdot type was determined in the different media to further characterize the Qdots and to quantify the observed quenching effects. The mean integrated fluorescence of 1 µM solutions of Qdot 620 ($4.3 \pm 0.6 \times 10^7$ A.U.) was significantly greater than the fluorescence for Qdot 520 ($1.8 \pm 0.1 \times 10^7$ A.U.; $P < 0.006$). Significant differences in the integrated fluorescence of the Qdots in the different media were also observed ($P = 0.01$), which suggests that the cell culture media components affect Qdot photoluminescence. No difference in the fluorescence was observed based on surface chemistry ($P = 0.28$) for either Qdot 520 or 620.

The percent quenching of Qdots in the different media was determined by dividing the integrated fluorescence of the Qdots in media by the integrated fluorescence in water (Table 1). The average percent quenching for Qdots 520 and 620 was 56 ± 3% and 57 ± 7%, respectively, and did not significantly vary based on size ($P = 0.90$). However, significant differences in quenching of the two culture media was observed ($P = 0.04$). DMEM10 and MEM15 media quenched Qdot fluorescence by 50 ± 4% and 63 ± 4%, respectively. These difference may be related to the increased amount of fetal bovine serum (FBS) in the MEM15 (15% PBS) as compared with DMEM10 (10% FBS). Adsorption of bovine serum albumin (BSA) to QDots has been shown to affect the quantum yield,[45,46] supporting this hypothesis. In addition, preliminary dynamic light scattering results (*not shown*) suggest significant aggregation of Qdots in cell culture media. Aggregation of Qdots is known to change the photoluminescent properties,[47] and may further affect the observed quenching in our experiments. Difference in the level of quenching between the two Qdot sizes (Qdot 520 = 56 ± 2%; Qdot 620 = 57 ± 2%) was not observed ($P = 0.90$). Qdots with NH_2-functionalized surfaces displayed a higher level of quenching (62 ± 4%) as compared to Qdots with COOH-functionalized surfaces (51 ± 4%); these difference, however, were not significant ($P = 0.123$).

Table 1. Qdot photoluminescence. Integrated fluorescence emission of the different Qdots in water and cell culture medium, and the quenching effects of the different media.

	Fluorescence (x 10^7 A.U.)	Media quenching (%)
520, COOH, Water	4.2	
520, COOH, DMEM10	2.0	53
520, COOH, MEM15	1.5	65
520, NH_2, Water	4.2	
520, NH_2, DMEM10	2.1	49
520, NH_2, MEM15	1.8	56
620, COOH, Water	10.4	
620, COOH, DMEM10	4.4	57
620, COOH, MEM15	3.0	72
620, NH_2, Water	9.8	
620, NH_2, DMEM10	5.9	39
620, NH_2, MEM15	4.0	59

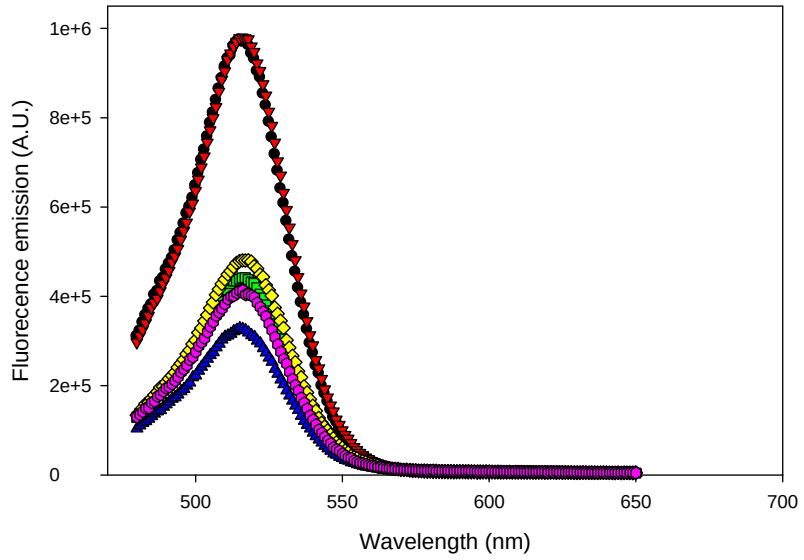

Figure 2. **Qdot 520 properties.** Fluorescence spectra of the Qdot 520, COOH and NH_2 surface, in water and cell culture media. ● – Qdot 520-COOH, water; ▼ – Qdot 520-NH_2, water; ■ – Qdot 520-COOH, DMEM10; ♦ – Qdot 520-NH_2, DMEM10; ▲ – Qdot 520-COOH, MEM15; ⬢ – Qdot 520-NH_2, MEM15.

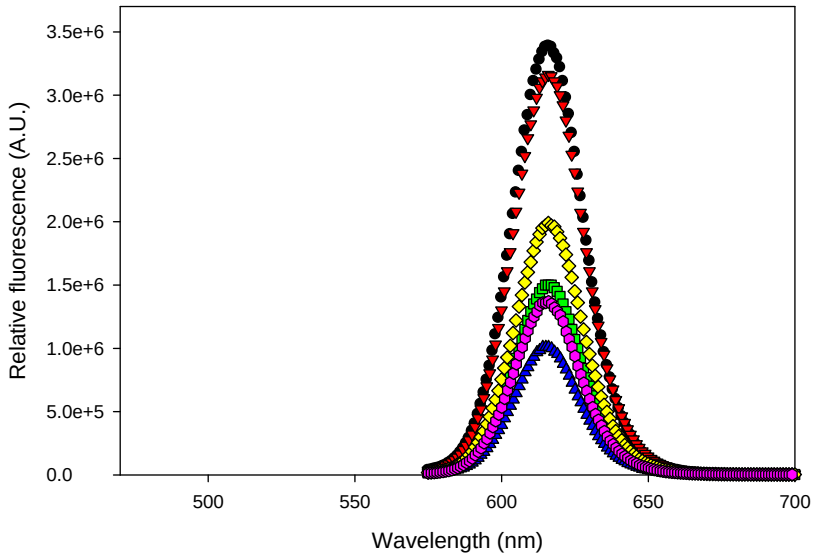

Figure 3. **Qdot 620 properties.** Fluorescence spectra of the Qdot 620, COOH and NH_2 surface, in water and cell culture media. ● – Qdot 620-COOH, water; ▼ – Qdot 620-NH_2, water; ■ – Qdot 620-COOH, DMEM10; ♦ – Qdot 620-NH_2, DMEM10; ▲ – Qdot 620-COOH, MEM15; ⬢ – Qdot 620-NH_2, MEM15.

3.2 Fluorescence localization and cell toxicity

Qdot uptake and localization

QDots of both sizes and surface chemistries (Qdot 520-NH_2 and -COOH; Qdot 620-NH_2 and –COOH) were internalized by RAW cells within 18 hours post-exposure (Figures 4-6). Qdot fluorescence was clearly visible in RAW cells exposed to 1 µM concentrations of Qdots 520 and 620, and 1 nM concentrations of Qdot 620. Fluorescence of Qdot 520 particles was observed at the 1 nM concentrations, but was considerable less distinct (Figure 4). Confocal imaging of RAW cells suggests that Qdots are internalized through endocytosis, and become distributed throughout the cytoplasm and perinuclear space (Figure 6). Previous reports have documented the endocytosis of Qdots and polystyrene nanoparticles coated with negatively charged COOH groups on the surface.[48,49] While Qdot aggregates have been observed within the nucleus,[50] localization of Qdots in the nucleus of RAW cells was not observed in our studies. The perinuclear distribution of Qdots within RAW cells suggests that they are localized within recycling endosomes. These observations are consistent with previous reports of endosomal localization of Qdots with both COOH and NH_2 surface groups.[48,49] In particular, RAW cells exposed to Qdot 620-NH_2 nanoparticles displayed greater perinuclear distribution than those exposed to Qdot 620-COOH nanoparticles (Figure 6). Confocal imaging also suggests that the Qdot 620 particles are internalized at a much greater level than the Qdot 520 particles.

The mean fluorescence of cells exposed to the different treatments was quantified to determine which parameters affected Qdot uptake in RAW cells (Figure 7A). A three-way interaction among Qdot size, surface chemistry, and concentration was observed in at 18 hours post-exposure, and a two-way interaction between Qdot size and concentration was observed at 42 hours post-exposure ($P < 0.001$; Table 2). Pairwise comparisons within the different treatments and time periods were performed using the Holm-Sidak method to further delineate significant effects. The mean relative fluorescence of RAW cells exposed to the 1 µM concentrations was significantly greater than control cells and those exposed to 1 nM concentrations of Qdots at both 18 and 42 hours. While Qdot fluorescence was visualized at the 1 nM concentrations, significant differences between the mean relative fluorescence of control cells and those exposed to 1 nM concentrations of Qdots were not observed (Table 3). This observation is due to variability in the percentage of cells with Qdots at the 1 nM treatment (Figure 7B). Approximately 80 – 100% of the RAW cells had fluorescence above the background level at the 1 µM concentrations of Qdots. In contrast, <30% of cells had Qdot fluorescence above the background level at the 1 nM concentrations. Together, these data suggest that, as expected, Qdot uptake is directly correlated with the concentration of Qdots, with greater uptake when the Qdot concentration is higher.

Significant differences in mean fluorescence based on size were observed at the 1 µM concentrations ($P < 0.01$; Table 3); differences based on size were not observed at the 1 nM concentrations. The mean fluorescence of RAW cells exposed to 1 µM Qdot 620-NH_2, but not Qdot 620-COOH, nanoparticles was significantly greater than that of cells exposed to Qdot 520 nanoparticles at 18 hours post-exposure, ($P < 0.01$; Figure 7A), suggesting that surface chemistry may also play an important role. At 42 hours post-exposure, however, the mean fluorescence of RAW cells exposed to 1 µM Qdot 620-NH_2 and Qdot 620-COOH, nanoparticles was significantly greater than that of cells exposed to the Qdot 520 nanoparticle treatments (Figure 7A). These data are consistent with observations from confocal imaging, which also suggest that the larger Qdot 620 nanoparticles are internalized to a greater extent than the Qdot 520 nanoparticles. While size-dependent uptake of 20 and 200 nm polymer nanoparticles has been reported,[48] similar effects have not been documented for Qdots. In our studies, internalization displays a size and concentration dependency, with the larger Qdots experiencing a greater level of uptake. These observations must be interpreted with caution as the shape, in addition to the size, may differ for Qdots with different emission spectra.[51] Differences in shape will affect the surface area of the Qdots, and likely how interactions with cell membranes may occur.

The three-way interaction observed at 18 hours post-exposure among Qdot size, surface chemistry, and concentration suggests that surface chemistry also played an important role in uptake (Table 3). Of all the treatments, a significant difference in uptake was observed only between 1 µM concentrations of Qdot 620-NH_2 and Qdot 620-COOH nanoparticles at 18 hours ($P < 0.01$); this difference was not observed at 42 hours post-exposure. Surface chemistry-dependent effects of Qdot uptake have been reported previously, and suggest that Qdots with negatively-charged (i.e., COOH) surfaces are more readily internalized than those with positively charged surfaces (i.e., NH_2).[48] In contrast, our studies suggest that the surface chemistry effects are considerably less than the size and concentration of Qdots with respect to cellular uptake. Further investigation will be critical to fully understanding the role of surface chemistry and uptake in RAW cells.

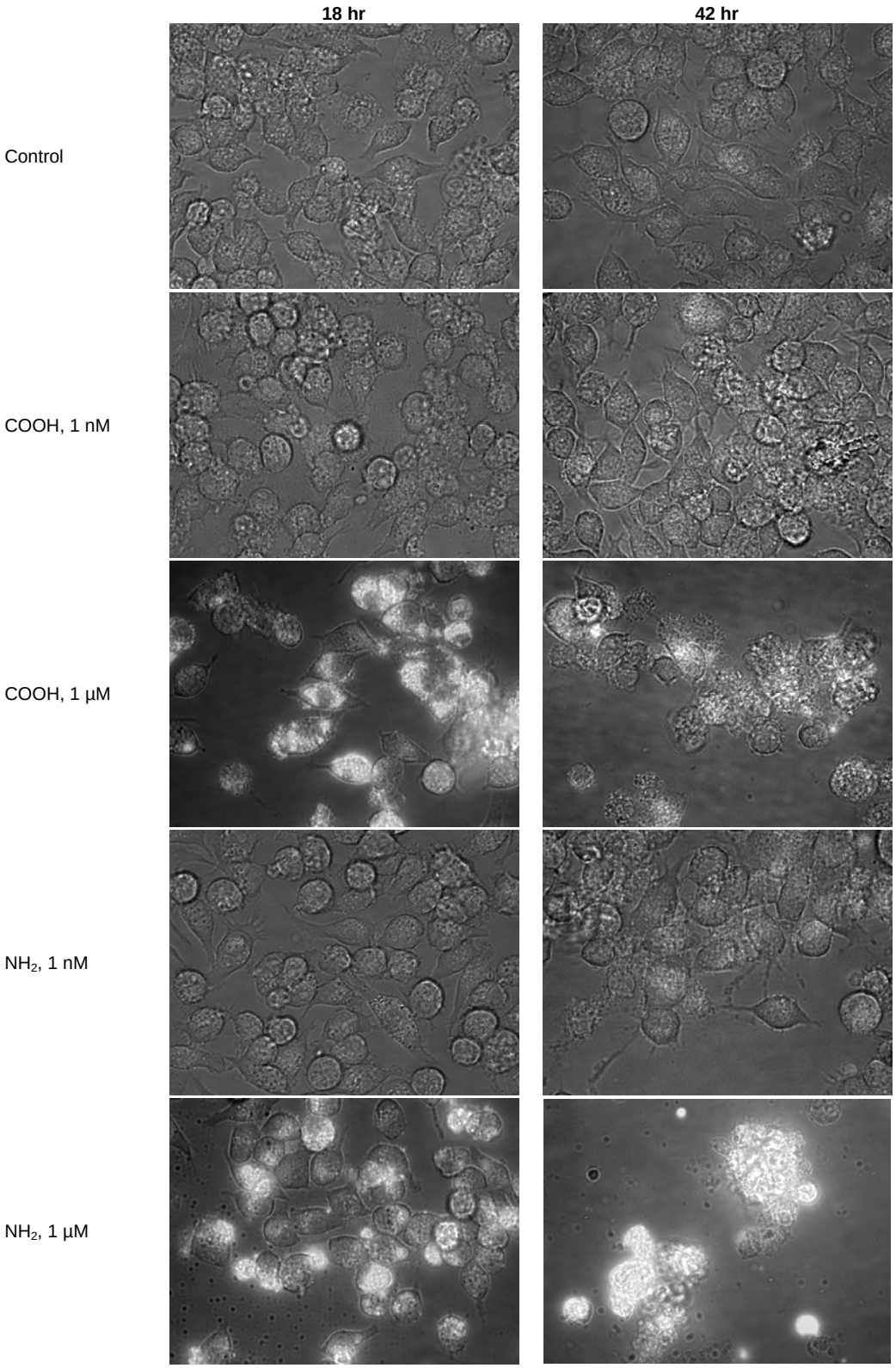

Figure 4. RAW-Qdot 520 imaging. Combined brightfield and fluorescence photomicrographs of RAW macrophage cells exposed to different treatments of Qdot 520 nanoparticles.

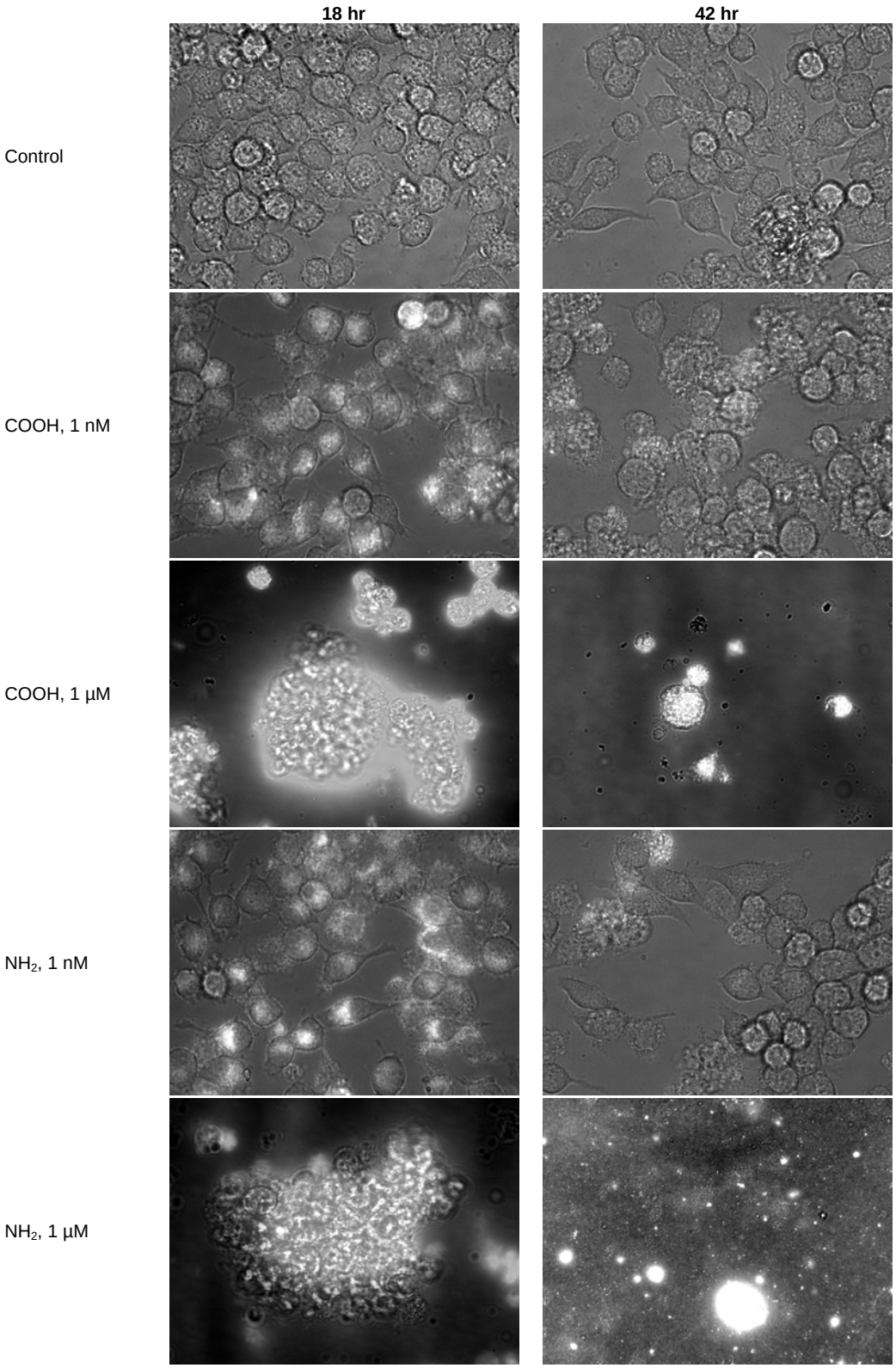

Figure 5. RAW-Qdot 620 imaging. Combined brightfield and fluorescence photomicrographs of RAW macrophage cells exposed to different treatments of Qdot 520 nanoparticles.

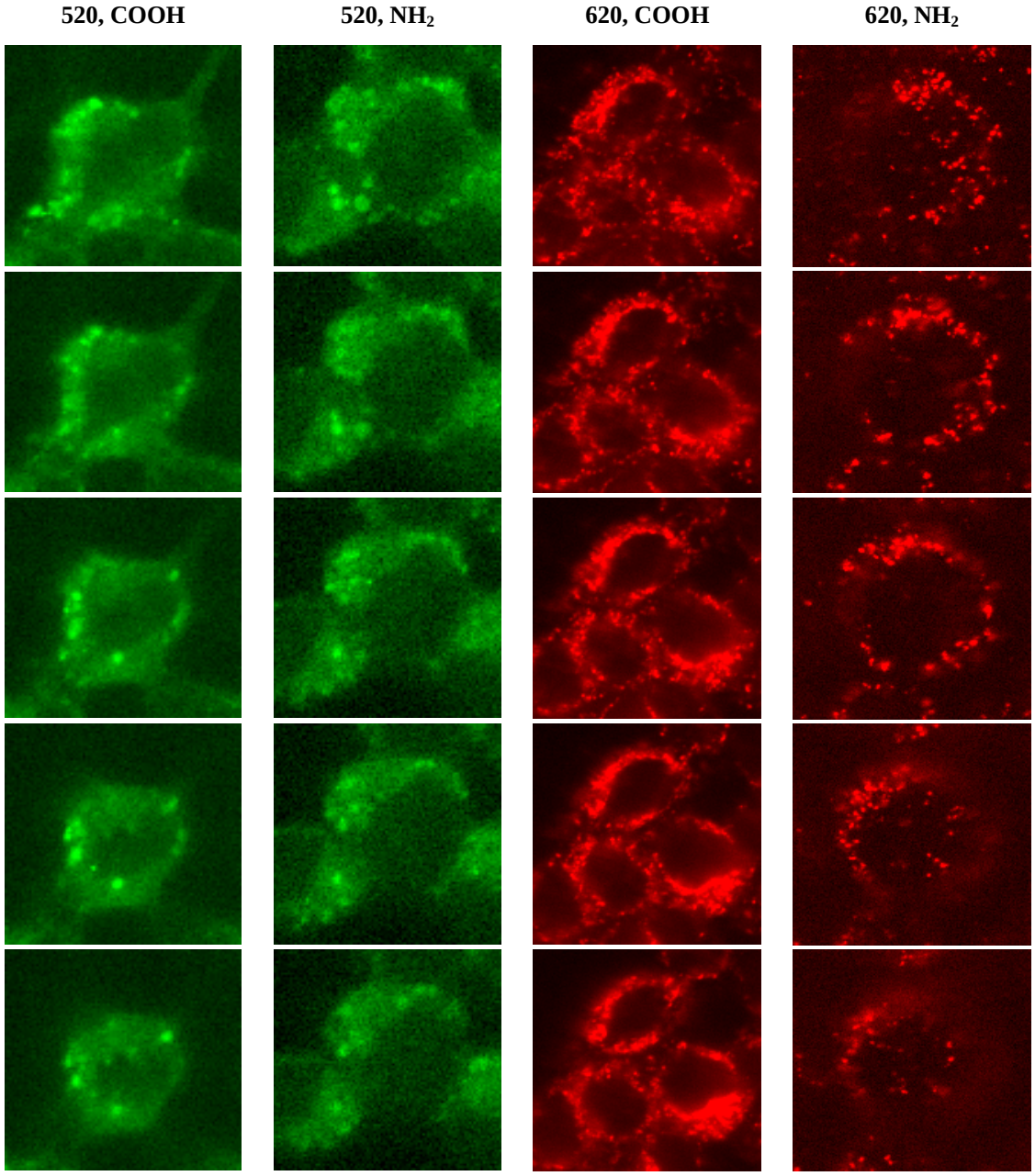

Figure 6. RAW-confocal imaging. Confocal z-slices of RAW macrophage cells exposed to 1 nM concentrations of QDot 520 and 620 nanoparticles with different surface chemistries (COOH and NH_2) at 18 hours post-exposure.

(A)

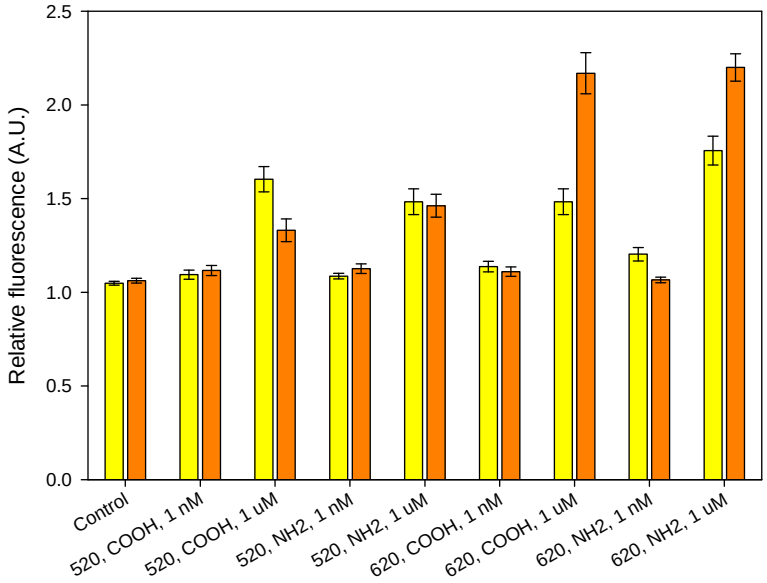

(B)

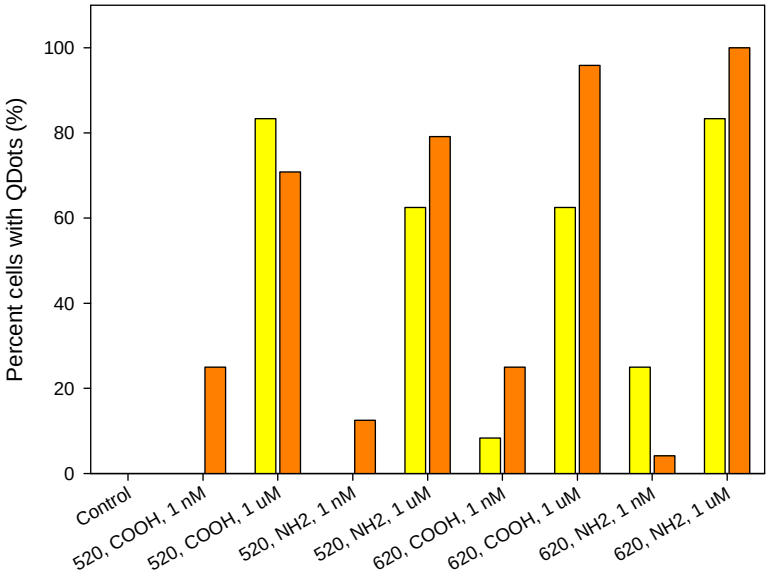

Figure 7. **RAW fluorescence results. (A)** Mean relative fluorescence (± standard error of the mean) of RAW cells at 18 (yellow bars) and 42 hours (orange bars) post-exposure to the different Qdot treatments. **(B)** Percent of RAW cells displaying fluorescence above background at 18 (yellow bars) and 42 hours (orange bars) post-exposure to the different Qdot treatments.

Table 2. Fluorescence ANOVA statistics. P-vales from Three-way ANOVA test of main effects and interactions of Qdot size, surface chemistry, and concentration on the relative fluorescence of RAW and RBL cells at 18 hr and 42 hr post-exposure. Values in bold text represent significant effects and interactions that are interpreted in the text.

	RAW		RBL	
	18 hr	42 hr	18 hr	42 hr
One-way effects				
Size	0.011	<0.001	<0.001	<0.001
Surface chemistry	0.088	0.351	0.902	<0.001
Concentration	<0.001	<0.001	<0.001	<0.001
Two-way effects				
Size x Surface chemistry	<0.001	0.258	0.860	0.003
Size x Concentration	0.134	**<0.001**	**<0.001**	<0.001
Surface chemistry x Concentration	0.279	0.209	0.011	<0.001
Three-way effects				
Size x Surface chemistry x Concentration	**<0.001**	0.625	0.717	**<0.001**

Table 3. Fluorescence – treatment effects. Pairwise comparisons of the relative fluorescence associated with the Qdot different treatments (i.e., size, surface chemistry, and concentration) at 18 and 42 hours in RAW and RBL cells.

	RAW		**RBL**	
	18 hr	**42 hr**	**18 hr**	**42 hr**
Concentration				
520, COOH, nM vs. Control	No	No	No	No
520, NH_2, nM vs. Control	No	No	No	No
620, COOH, nM vs. Control	No	No	Yes	Yes
620, NH_2, nM vs. Control	No	No	Yes	No
520, COOH, µM vs. Control	Yes	Yes	Yes	Yes
520, NH_2, µM vs. Control	Yes	Yes	Yes	Yes
620, COOH, µM vs. Control	Yes	Yes	Yes	Yes
620, NH_2, µM vs. Control	Yes	Yes	Yes	Yes
520, COOH, µM vs. 520, COOH, nM	Yes	No	Yes	No
520, NH_2, µM vs. 520, NH_2, nM	Yes	Yes	Yes	Yes
620, COOH, µM vs. 620, COOH, nM	Yes	Yes	Yes	Yes
620, NH_2, µM vs. 620, NH_2, nM	Yes	Yes	Yes	Yes
Size				
520, COOH, nM vs. 620, COOH, nM	No	No	Yes	No
520, COOH, µM vs. 620, COOH, µM	No	Yes	Yes	Yes
520, NH_2, nM vs. 620, NH_2, nM	No	No	Yes	No
520, NH_2, µM vs. 620, NH_2, µM	Yes	Yes	Yes	Yes
Surface chemistry				
520, NH_2, nM vs. 520, COOH, nM	No	No	No	No
520, NH_2, µM vs. 520, COOH, µM	No	No	No	Yes
620, NH_2, nM vs. 620, COOH, nM	No	No	No	No
620, NH_2, µM vs. 620, COOH, µM	Yes	No	No	No

RBL cells readily interacted with all Qdot treatments (Figures 8 and 9), but displayed minimal internalization of Qdots (Figure 10). The overall fluorescence was greater for RBL cells exposed to the Qdot 620 treatments as compared with Qdot 520 nanoparticles (Figure 11A), which is similar to observations for RAW cells. Confocal imaging of RBL cells, however, suggests that internalization was substantially less than observed with RAW cells at 18 hours after exposure. RBL cells exposed to the Qdots have mainly a membrane-associated distribution, with limited (if any) cytoplasmic distribution. Endocytosis in RBL cells is mediated through membrane receptors.[52] The lack of internalization suggests that Qdots did not interact with the FcεRI complexes in a manner that enables uptake. Differences in the distribution of Qdots on RBL cell membranes also differed based on the Qdot size. Cells exposed to the Qdot 620 treatments displayed a higher level of association and a uniform distribution on the membrane surface. In contrast, the association of Qdot 520 nanoparticles with the cell membrane was much lower and displayed an aggregated distribution (Figure 10).

A two-way interaction between Qdot size and concentration was observed in at 18 hours post-exposure, and a three-way interaction among Qdot size, surface chemistry, and concentration was observed at 42 hours post-exposure in RBL cells ($P < 0.001$; Table 2). The mean relative fluorescence of RBL cells exposed to the 1 µM concentrations was significantly greater than control cells and those exposed to 1 nM concentrations of Qdots at both 18 and 42 hours (Table 3). Significant differences in the mean fluorescence of cells exposed to the 1 nM concentrations of Qdot 620-COOH were observed at 18 and 42 hours exposure, and 1 nM concentration of Qdot 620-NH_2 at 18 hours post-exposure (Table 3). As observed with RAW cells, the percent of RBL cells with Qdots varied considerably by treatment (Figure 10B), principally when cells were exposed at the 1 nM concentrations. For example, ~10% of RBL cells had a mean fluorescence above background at the 1 nM concentration of Qdot 520-COOH, as compared with ~50% of cells exposed to the Qdot 620-COOH. Overall, these data suggest that Qdot association with RBL cell membranes is, as expected, highly dependent on the concentration of exposure.

Size-dependent differences in mean fluorescence of RBL cells were observed at the 1 µM concentrations of Qdots at 18 and 42 hours post-exposure ($P < 0.01$; Table 3); significant size-dependent differences were at the 1 nM concentrations of Qdots were observed only at 18 hours post-exposure. In these treatments, the mean fluorescence was significantly greater for all Qdot 620 treatments (Table 3), which agrees with observations from the confocal imaging. Similarly, the percent of RBL cells with Qdot fluorescence above background was higher in all Qdot 620 treatments as compared with Qdot 520 nanoparticles (Figure 11B). Together these data suggest that Qdot size is a critical factor affecting the association of these nanoparticles with cell membranes. As noted earlier, this size-dependent relationship must be interpreted with caution as shape differences may also exist,[51] and affect how Qdots interact with cell membranes. This issue is particularly important for RBL cells based on the high degree of Qdot association with cell membranes and protein components.

The three-way interaction in the mean fluorescence was observed in RBL cells at 42 hours post-exposure among Qdot size, surface chemistry, and concentration (Table 3), which suggests that surface chemistry may also play an important role. Of all the treatments, a significant difference in fluorescence was only observed between 1 µM concentrations of Qdot 520-NH_2 and Qdot 520-COOH nanoparticles at 42 hours ($P < 0.01$); this difference was not observed at 18 hours post-exposure. Because Qdots are primarily associated with the RBL membranes, surface chemistry (negatively versus positively charged surfaces) should play an important role controlling the interactions between the Qdots and the charged domains in membrane proteins. The relatively limited differences, however, suggest that surface chemistry plays only a minor role in driving interactions between Qdots and RBL cell membrane, as compared with the effects of size and concentration.

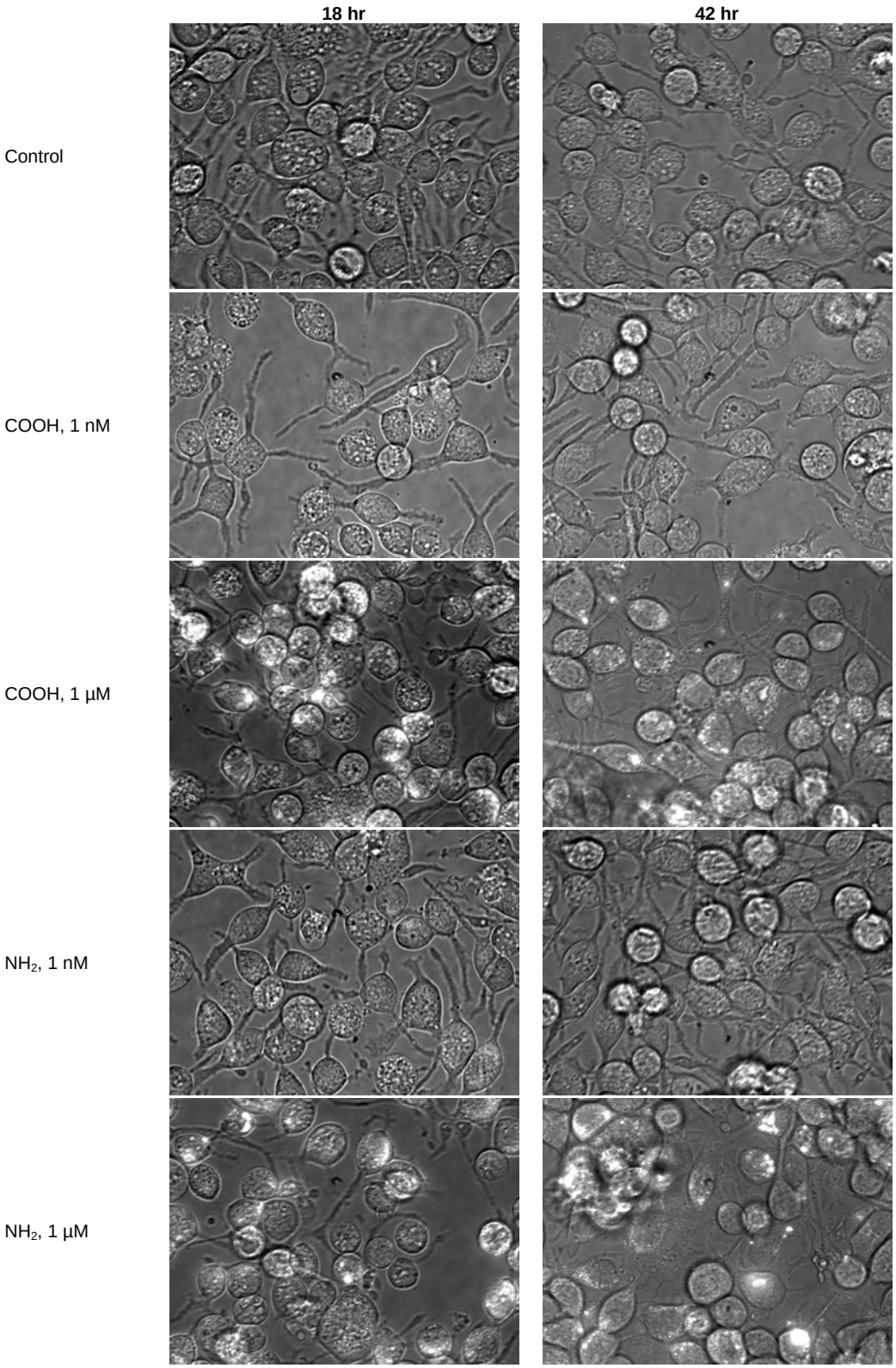

Figure 8. RBL-Qdot 520 imaging. Combined brightfield and fluorescence photomicrographs of RBL mast cells exposed to different treatments of Qdot 520 nanoparticles.

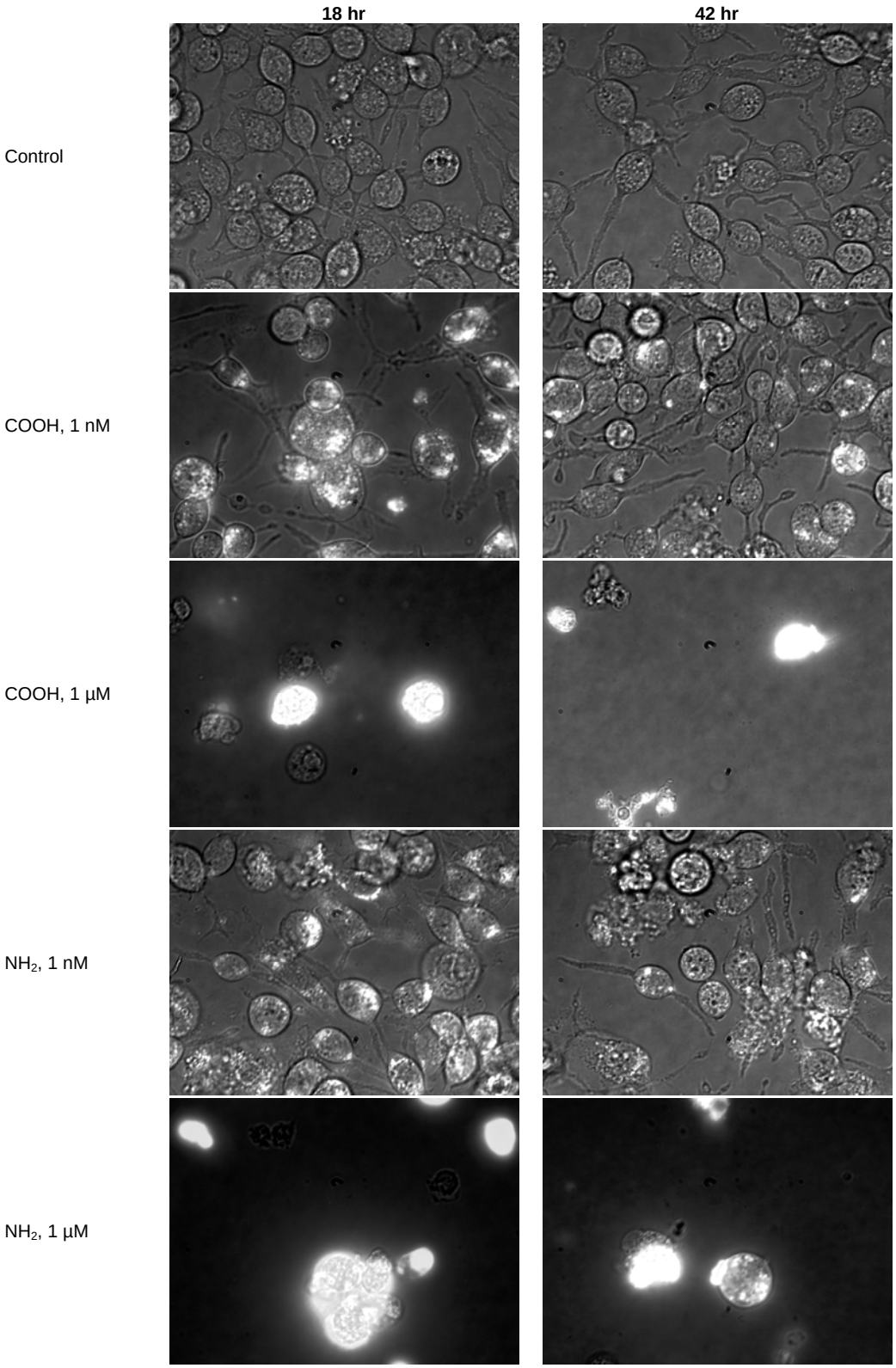

Figure 9. RBL-Qdot 620 imaging. Combined brightfield and fluorescence photomicrographs of RBL mast cells exposed to different treatments of Qdot 620 nanoparticles.

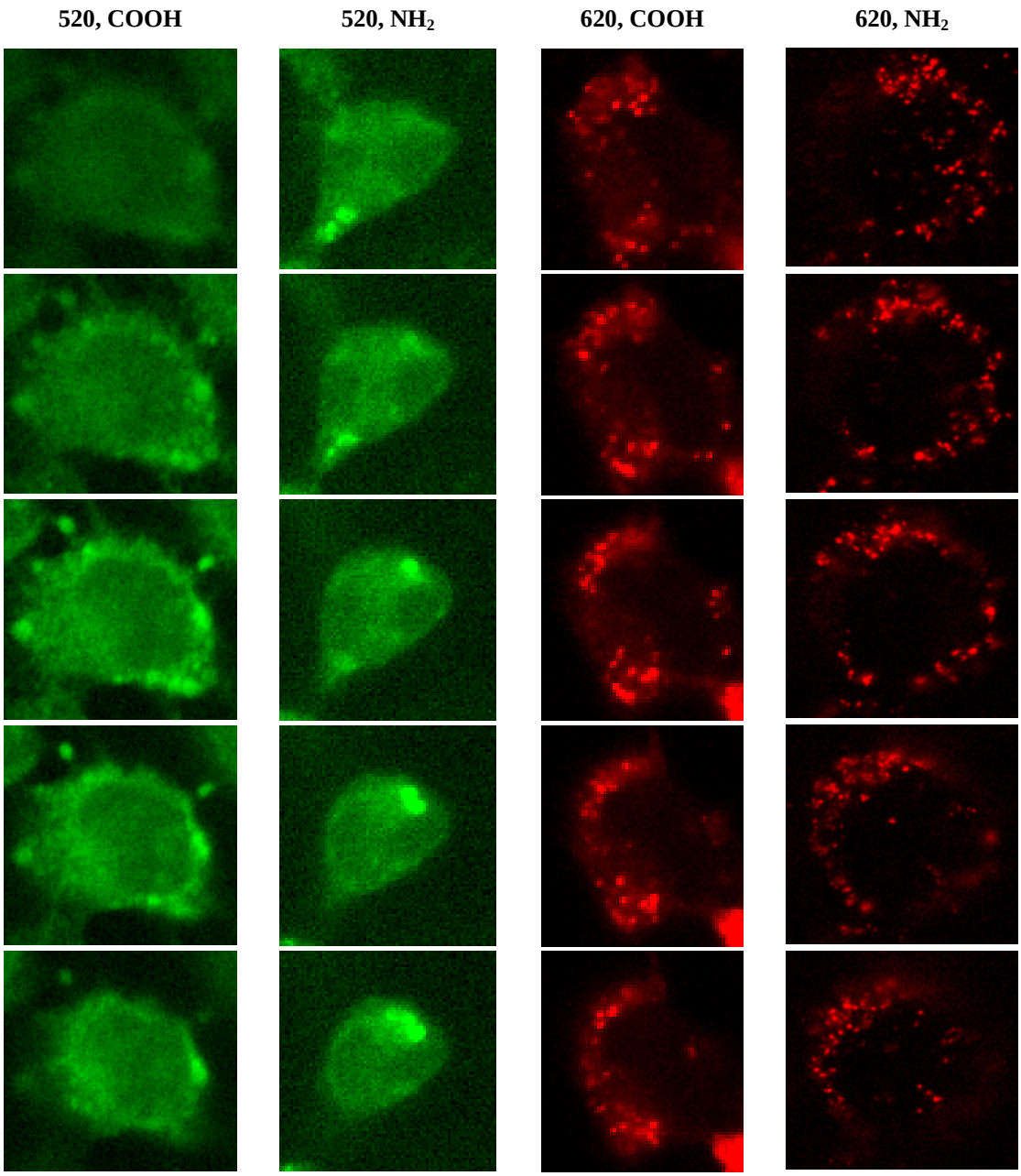

Figure 10. RBL-confocal imaging. Confocal z-slices of RAW macrophage cells exposed to 1 nM concentratrions of QDot 520 and 620 nanoparticles with different surface chemistries (COOH and NH_2) at 18 hours post-exposure.

(A)

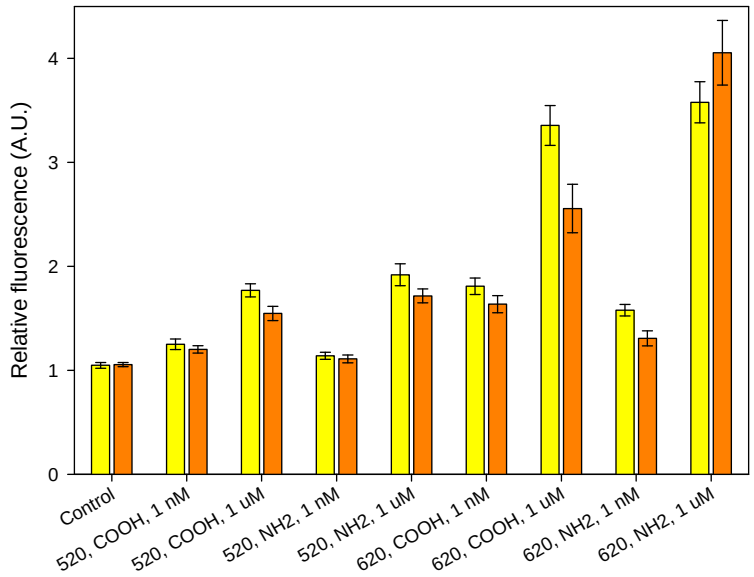

(B)

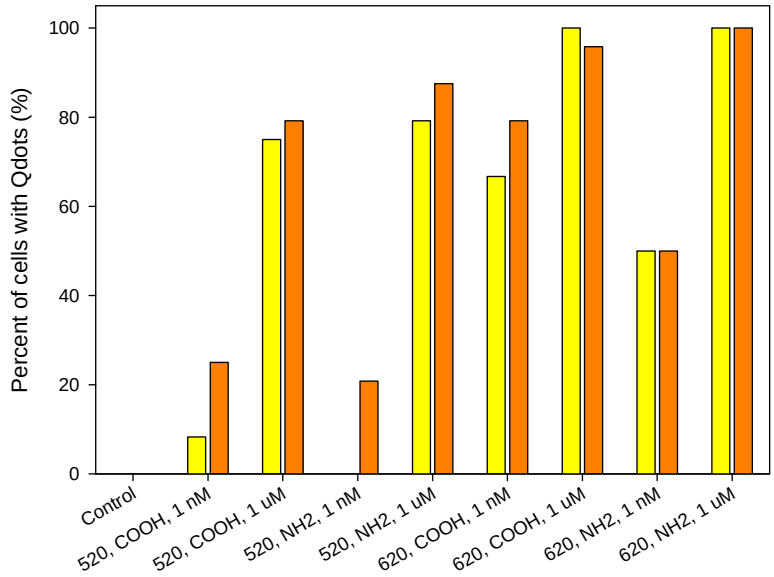

Figure 11. RBL fluorescence results. (A) Mean relative fluorescence (± standard error of the mean) of RBL cells at 18 (yellow bars) and 42 hours (orange bars) post-exposure to the different Qdot treatments. **(B)** Percent of RBL cells displaying fluorescence above background at 18 (yellow bars) and 42 hours (orange bars) post-exposure to the different Qdot treatments.

Toxicity

The confluency of RAW and RBL cell cultures was significantly affected by the different Qdot treatments (Figure 12). The confluency of control RAW cells (i.e., not exposed to Qdots) was constant (~70%) at 18 and 42 hours post-exposure, but significantly affected by the Qdot treatments at both time points ($P < 0.001$; Table 4). Significantly lower levels of confluency were observed for RAW cells exposed to the 1 μM concentrations of Qdot 620-COOH and Qdot 620-NH_2 nanoparticles, as compared with control cells at 18 hours (Figure 11A; Table 5). Similarly, a two-way interaction between size and concentration was observed at 42 hours post-exposure for RAW cells (Table 5). The significantly lower confluency levels of RAW cells exposed to the 1 μM concentrations of Qdot 620-COOH and Qdot 620-NH_2 nanoparticles were also observed at 42 hours post-exposure (Table 6). In addition, a significant difference between Qdot 520-COOH and Qdot 620-COOH nanoparticles was observed, suggesting that toxicity is size-dependent. Overall, these data are consistent with the size-dependent relationship observed for Qdot uptake in RAW cells, and indicate that cytotoxicity is directly correlated with Qdot uptake. Size-dependent toxicity has been observed for CdTe Qdot, but suggest that the toxicity is inversely proportional to size.[53] Direct comparison of the results, however, are difficult as the core materials and surface coatings are substantially different from those used in our study. Reports also suggest that Qdot-induced toxicity is dependent on the surface chemistry, but are conflicting with respect to whether positively- or negatively charged (NH_2) surfaces induce greater toxicity. [48,50] Our data suggest that the cytotoxicity of Qdots in RAW cells is affected by surface chemistry, which is similar to observations for Qdot-induced cytotoxicity in kidney cells.[54]

A significant decrease in the confluency of RBL cells was also observed based on Qdot exposure (Figure 12B). As observed with RAW cells, significant two-way interactions between the QDot size and concentration were observed at both 18 and 42 hours post-exposure (Table 5; $P < 0.001$). RBL cells exposed to 1 μM concentrations of Qdot 620-COOH and Qdot 620-NH_2 nanoparticles displayed a significant decrease in confluency at both 18 and 42 hours post-exposure ($P < 0.001$), whereas no change in the confluency was for Qdot 520 treatments (Figure 12B). The confluency of RBL cells was not affected by surface chemistry at either 18 or 42 hours post-exposure. These results are consistent with the observations for RAW cells in which the larger, red Qdots induced a higher level of cytotoxicity. A critical distinction, however, must be made with respect to the cytotoxic affects observed in these two cells lines. Confocal imaging suggests that Qdot are internalized by RAW cells through endocytosis, whereas Qdots associate primarily with RBL cell membranes and experience very little uptake. Thus, the observed cytotoxicity in RBLs is induced through fundamental interactions between Qdots and the cell membrane and membrane proteins. Because the Qdots do not enter the cell, Qdot-induced toxicity must proceed through routes that are discrete from those reported for internalized Qdots. The ability of Qdots to form pores and enable bursts of ion current to flow across cell membranes has been demonstrated,[55] and represents a route for the cytotoxic response observed in RBL cells. Qdots may also bind electrostatically to proteins, such as ion channels, in the cell membrane and disrupt physiological function.

Overall, our data demonstrate that Qdot-induced toxicity is dependent on size and concentrations, and shows minimal dependency on the surface charge of the polymer coating. Cytotoxicity was significantly greater for RAW and RBL cells exposed to the larger, Qdot 620 nanoparticles, independent of the surface functionalization. In addition, cytotoxicity is not limited to cells in which QDots are internalized. Substantial cytotoxicity was observed in RBL cells in which the Qdots were uniformly distributed on the surface of the cell membrane. Further investigation is needed to fully understand the mechanisms by which toxicity is induced (e.g., necrosis versus apoptosis) when Qdots are exclusively bound to the membrane, as compared to when Qdots are internalized. Understanding these mechanisms is critical to predicting the toxicity of new nanoparticles based on their fundamental interactions with cells.

(A)

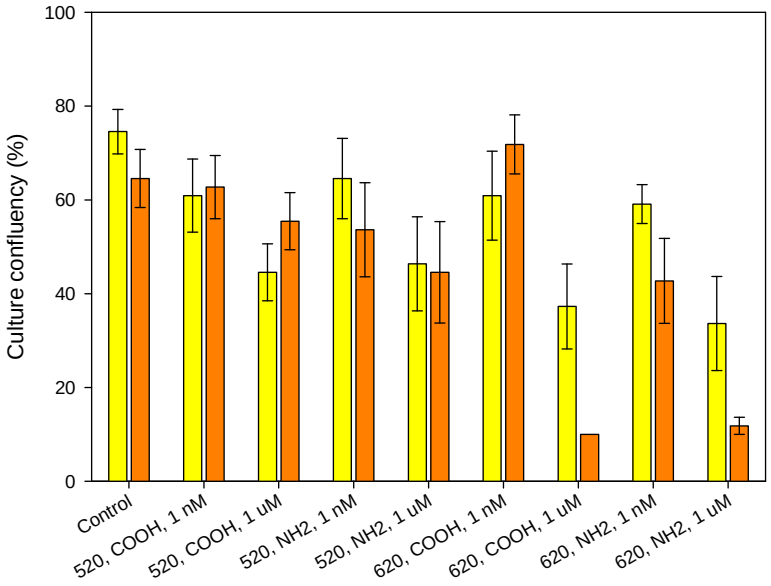

(B)

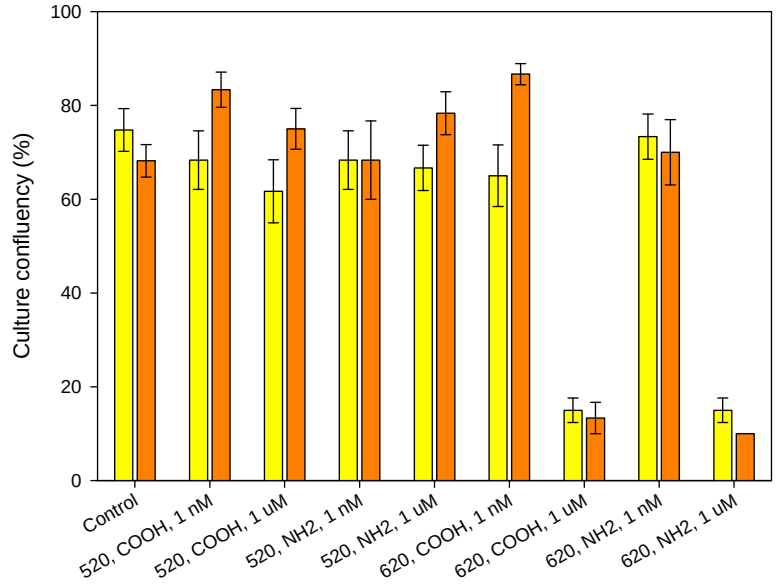

Figure 12. **RAW and RBL toxicity.** Confluency of RAW (**A**) and RBL **(B**) cell cultures at 18 (yellow bars) and 42 hours (orange bars) post-exposure to the different Qdot treatments. Error bars are the standard error of the mean.

Table 4. Confluency ANOVA statistics. P-vales from Three-way ANOVA test of single and multiple interaction effects of Qdot size, surface chemistry, and concentration on the confluency of RAW and RBL cell cultures. Values in bold text represent significant effects and interactions that are interpreted in the text.

	RAW		RBL	
	18 hr	42 hr	18 hr	42 hr
One-way effects				
Size	0.289	0.002	<0.001	<0.001
Surface chemistry	1.00	0.066	0.464	0.065
Concentration	**<0.001**	<0.001	<0.001	<0.001
Two-way effects				
Size x Surface chemistry	0.649	0.776	0.855	0.625
Size x Concentration	0.588	**<0.001**	**<0.001**	**<0.001**
Surface chemistry x Concentration	0.986	0.156	0.833	0.032
Three-way effects				
Size x Surface chemistry x Concentration	0.937	0.352	0.701	0.882

Table 5. Confluency – treatment effects. ANOVA results for the comparison of the different QDot treatments (i.e., size, surface chemistry, and concentration) at 18 and 42 hours of RAW and RBL cells exposed to QDots.

	RAW		**RBL**	
	18 hr	**42 hr**	**18 hr**	**42 hr**
Concentration				
520, COOH, nM vs. Control	No	No	No	No
520, NH_2, nM vs. Control	No	No	No	No
620, COOH, nM vs. Control	No	No	No	No
620, NH_2, nM vs. Control	No	No	No	No
520, COOH, µM vs. Control	No	No	No	No
520, NH_2, µM vs. Control	No	No	No	No
620, COOH, µM vs. Control	Yes	Yes	Yes	Yes
620, NH_2, µM vs. Control	Yes	Yes	Yes	Yes
520, COOH, µM vs. 520, COOH, nM	No	No	No	No
520, NH_2, µM vs. 520, NH_2, nM	No	No	No	No
620, COOH, µM vs. 620, COOH, nM	No	Yes	Yes	Yes
620, NH_2, µM vs. 620, NH_2, nM	No	No	Yes	Yes
Size				
520, COOH, nM vs. 620, COOH, nM	No	No	No	No
520, COOH, µM vs. 620, COOH, µM	No	Yes	Yes	Yes
520, NH_2, nM vs. 620, NH_2, nM	No	No	No	No
520, NH_2, µM vs. 620, NH_2, µM	No	No	Yes	Yes
Surface chemistry				
520, NH_2, nM vs. 520, COOH, nM	No	No	No	No
520, NH_2, µM vs. 520, COOH, µM	No	No	No	No
620, NH_2, nM vs. 620, COOH, nM	No	No	No	No
620, NH_2, µM vs. 620, COOH, µM	No	No	No	No

3.3 Changes in cytokine and superoxide dismutase levels

Changes in cytokine release

Changes in cytokine production and excretion are important signs of an inflammatory response to pathogen invasion and/or exposure to xenobiotics. Changes in the cytokines IL-10 and TNF-α, and IL-4 and TNF-α were characterized in RAW and RBL cells, respectively, to assess up-regulation of inflammatory response pathways due to Qdot exposure. A significant increase in TNF-α and decrease in IL-10 was observed in RAW cells exposed to the 1 μM concentrations of all Qdot treatments, but not those exposed to the 1 nM concentrations of Qdots (Figure 13). A three-way interaction among size, concentration, and surface chemistry was observed for the levels of TNF-α (Table 6). Size- and surface chemistry-dependent difference were observed between the 1 μM concentrations of the Qdot 520-COOH and Qdot 620-COOH treatments, and 1 μM concentrations of the Qdot 520-COOH and Qdot 520-NH_2 treatments, respectively (Table 7). Of all treatments, the Qdot 520-COOH nanoparticles induced the greatest increase in TNF-α release (Figure 13A). TNF-α stimulates neutrophil proliferation during an inflammatory response, and thus suggests that the high concentrations of Qdots induced a pro-inflammatory response. A concentration-dependent main effect was observed for IL-10 in RAW cells (Table 6), in which all 1 μM concentrations of Qdot treatments displayed a significant decrease in IL-10 release as compared with the control cells (Table 7; Figure 13B). No change in IL-10 levels was observed for the 1 nM concentrations of Qdots. IL-10 has an anti-inflammatory impact on many types of immune cells (e.g., neutrophils). Thus, the decreased levels of IL-10 further confirmed a pro-inflammatory response of RAW cells to Qdots. A two-dimensional plot of the changes in TNF-α and IL-10 concentrations displayed two clusters representing the two concentrations of Qdots (Figure 14), and showing the inverse correlation between the changes in TNF-α and IL-10 release. Similar changes in cytokine production and pro-inflammatory responses have been reported in response to Qdots exposure in epidermal keratinocytes, where changes in IL-1 beta, IL-6, and IL-8 release were observed for negatively charged (COOH), but not positively charged (NH_2) Qdots.[50] Together, these data suggest that RAW cells exhibit a pro-inflammatory response and related changes in cytokine release in response to high concentrations of Qdots. Limited size- and surface chemistry-dependent effects were observed in cytokine response, and require additional investigation to fully understand these relationships.

Changes in TNF-α and IL-4 concentrations were also observed in RBL cells exposed to Qdots (Figure 15). A two-way interaction between size and concentration was observed with respect to changes in TNF-α (Table 6). Whereas TNF-α release was up-regulated in RAW cells, RBL cells exposed to the 1 μM concentrations of Qdots experienced significant decreases in TNF-α release as compared with the control treatments (Table 7). In contrast, an increase in TNF-α release was observed in RBL cells at the 1 nM concentrations of Qdot 620-COOH and Qdot 620-NH_2; only the change observed for the Qdot 620-NH_2, however, was significant as compared with control cells (Table 7). A size-dependent difference in TNF-α level was also detected between the 1 nM treatments of Qdot 620-NH_2 and Qdot 520-NH_2 (Table 7). Overall, the data suggest that TNF-α release from RBL cells was substantially suppressed at high concentrations of Qdots. This suppression may be related to the membrane-based association of Qdots in RBL cells that was observed by fluorescence and confocal microscopy. Electrostatic interactions between Qdots and membrane receptors and channels may inhibit the ability of RBL cells to effectively release TNF-α in response to Qdot exposure. Based on this proposed mechanism, the inhibition should be concentration dependent and be reduced at lower Qdot concentrations. The increased levels of TNF-α observed at the 1 nM treatments of Qdot 620 nanoparticles supports this hypothesis as a possible mechanism for suppressing TNF-α release. The levels of IL-4 release were also affected by Qdot exposure (Figure 15B), and displayed a two-way interaction between size and concentration (Table 7). As observed with TNF-α in RBL cells, significant decreases in IL-4 release were observed for the 1 μM treatments of Qdot 620-COOH and Qdot 620-NH_2 (Table 7). The Qdot 520 nanoparticles did not induce changes in IL-4, suggesting that there is a size-dependency on the suppression of IL-4 release. It is important, however, to note that the observed changes in IL-4 were relatively minor in magnitude (i.e., < 1 pg/mL) and should be interpreted with a degree of caution. A two-dimensional plot of changes in TNF-α and IL-4 concentrations displayed two clusters representing the two concentrations of Qdots (Figure 16), similar to that observed for RAW cells. The RBL clusters, however, suggest that both IL-4 and TNF-α release are suppressed by the 1 μM concentrations of Qdots, which may be directly related to the association of Qdots with the RBL cell membrane and associated receptors and channels. Additional analysis of intracellular proteins involved in the inflammatory response, however, is needed to fully discern whether the observed changes in cytokines are due to down-regulation in production or suppression of cytokine release.

(A)

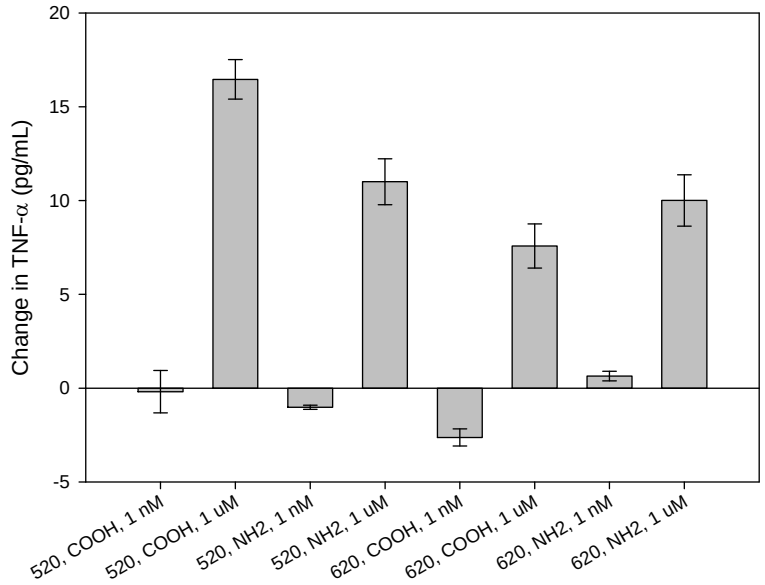

(B)

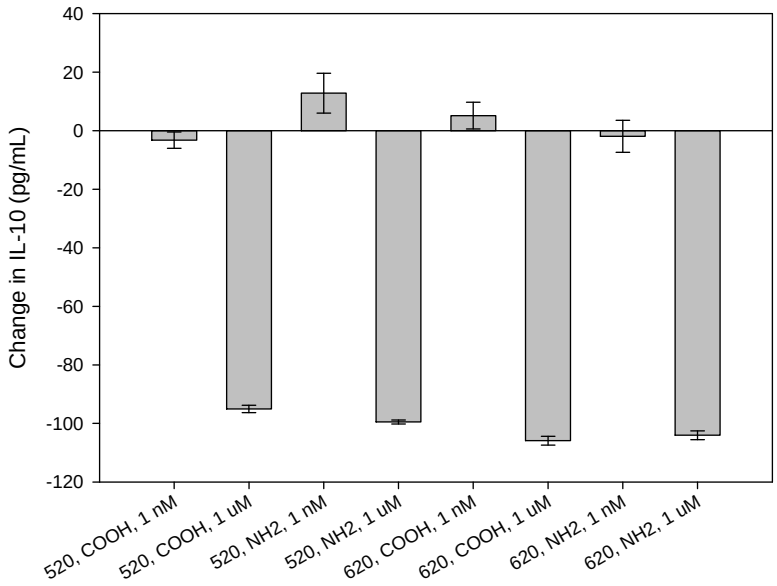

Figure 13. **RAW cytokine results.** Changes in the levels of (**A**) TNF-α and (**B**) IL-10 measured from RAW macrophage cells at 18 hours after exposure to the different types of QDots. Values represent changes compared to control RAW cells not exposed to Qdots. Error bars are the standard error of the mean.

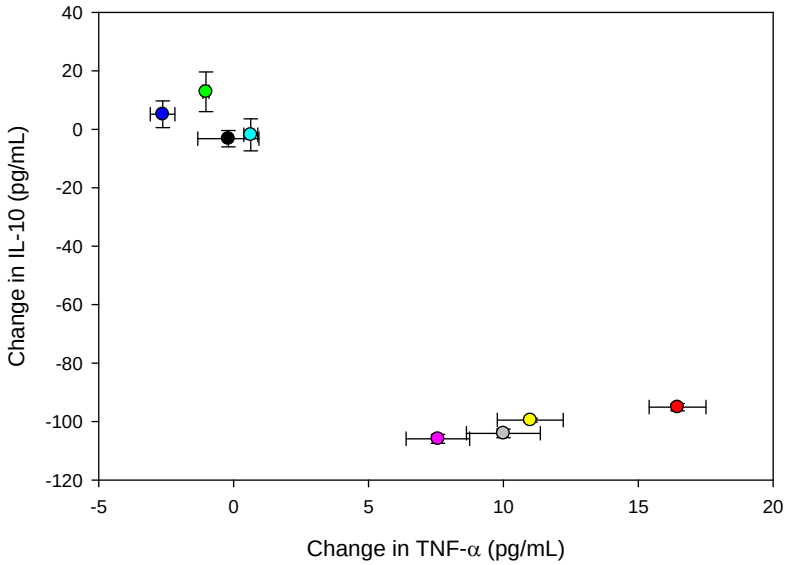

Figure 14. **RAW – 2D cytokine plot.** Concentrations of TNF-α and IL-10 in RAW macrophage cells at 18 hours after exposure to the different treatments of QDots. Symbols: 520-COOH-nM (●), 520-COOH-µM (●), 520-NH_2-nM (●), 520-NH_2-µM (●), 620-COOH-nM (●), 620-COOH-µM (●), 620-NH_2-nM (●), and 620-NH_2-µM (●). Error bars are the standard error of the mean.

Table 6. Cytokine ANOVA statistics. P-vales from Three-way ANOVA test of single and multiple interaction effects of Qdot size, surface chemistry, and concentration on the levels of TNF-α and IL-10 in RAW macrophage cells, and TNF-α and IL-4 in RBL mast cells. Values in bold text represent significant effects and interactions that are interpreted in the text.

	RAW		RBL	
	TNF-α	IL-10	TNF-α	IL-4
One-way effects				
Size	0.005	0.256	0.052	<0.001
Surface chemistry	0.869	0.737	0.174	0.454
Concentration	<0.001	**<0.001**	<0.001	<0.001
Two-way effects				
Size x Surface chemistry	0.002	0.380	0.509	0.427
Size x Concentration	0.003	0.576	**<0.001**	**<0.001**
Surface chemistry x Concentration	0.242	0.763	0.018	0.863
Three-way effects				
Size x Surface chemistry x Concentration	**0.022**	0.185	0.468	0.845

Table 7. Cytokine – treatment effects. ANOVA results for the comparison of the different Qdot treatments (i.e., size, surface chemistry, and concentration) on cytokine expression in RAW and RBL cells exposed to QDots.

	RAW		**RBL**	
	TNF-α	**IL-10**	**TNF-α**	**IL-10**
Concentration				
520, COOH, nM vs. Control	No	No	No	Yes
520, NH_2, nM vs. Control	No	No	No	No
620, COOH, nM vs. Control	No	No	No	No
620, NH_2, nM vs. Control	No	No	Yes	No
520, COOH, µM vs. Control	Yes	Yes	Yes	No
520, NH_2, µM vs. Control	Yes	Yes	Yes	No
620, COOH, µM vs. Control	Yes	Yes	Yes	Yes
620, NH_2, µM vs. Control	Yes	Yes	Yes	Yes
520, COOH, µM vs. 520, COOH, nM	Yes	Yes	Yes	No
520, NH_2, µM vs. 520, NH_2, nM	Yes	Yes	Yes	No
620, COOH, µM vs. 620, COOH, nM	Yes	Yes	Yes	Yes
620, NH_2, µM vs. 620, NH_2, nM	Yes	Yes	Yes	Yes
Size				
520, COOH, nM vs. 620, COOH, nM	No	No	No	No
520, COOH, µM vs. 620, COOH, µM	Yes	No	No	Yes
520, NH_2, nM vs. 620, NH_2, nM	No	No	Yes	No
520, NH_2, µM vs. 620, NH_2, µM	No	No	No	Yes
Surface chemistry				
520, NH_2, nM vs. 520, COOH, nM	No	No	No	No
520, NH_2, µM vs. 520, COOH, µM	Yes	No	No	No
620, NH_2, nM vs. 620, COOH, nM	No	No	No	No
620, NH_2, µM vs. 620, COOH, µM	No	No	No	No

(A)

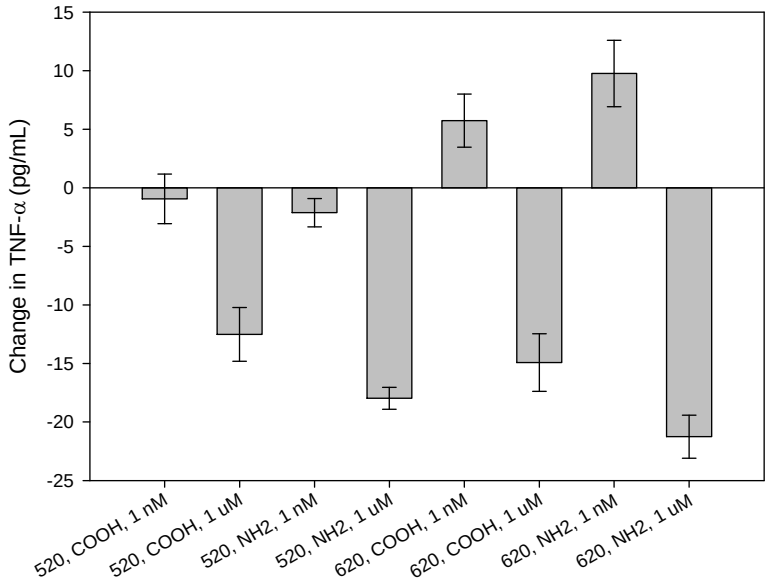

(B)

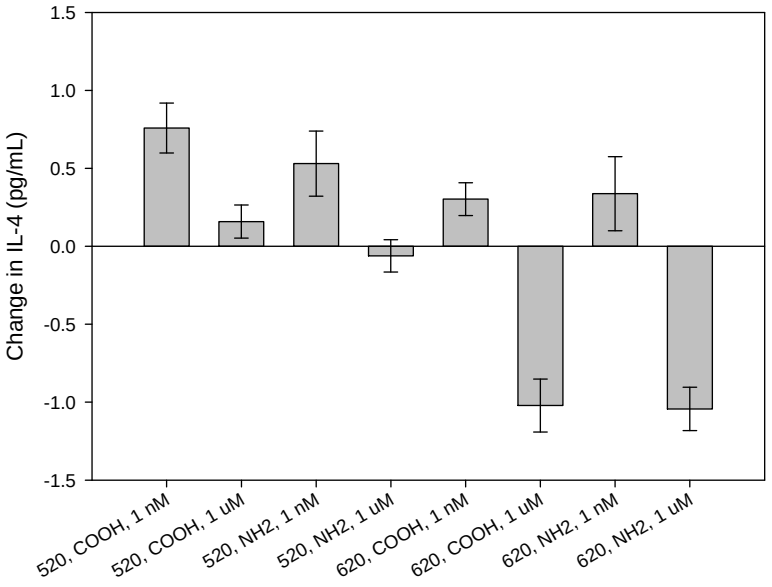

Figure 15. RBL cytokine results. Changes in the levels of (**A**) TNF-α and (**B**) IL-4 measured from RBL mast cells at 18 hours after exposure to the different types of QDots. Values represent changes compared to control RAW cells not exposed to Qdots. Error bars are the standard error of the mean.

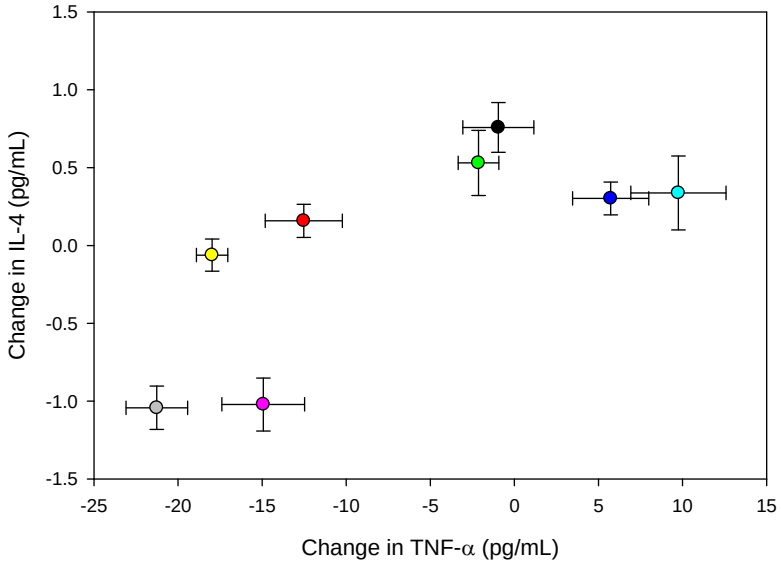

Figure 16. **RBL – 2D cytokine plot.** Concentrations of TNF-α and IL-4 in RBL mast cells at 18 hours after exposure to the different treatments of QDots. Symbols: 520-COOH-nM (●), 520-COOH-µM (●), 520-NH_2-nM (●), 520-NH_2-µM (●), 620-COOH-nM (●), 620-COOH-µM (●), 620-NH_2-nM (●), and 620-NH_2-µM (●). Error bars are the standard error of the mean.

Changes in superoxide dismutase levels

Increased levels of oxidative stress have been observed in cells exposed to single-walled carbon nanotubes[56] and Qdots.[57] Such physiological effects can lead to serious damage to proteins and DNA, and induce cell death. Cells mediate oxidative stress using enzymes such as superoxide dismutase, which catalyzes the dismutation of superoxides into oxygen and hydrogen peroxide. Changes in the activity of such enzymes may be characterized as indicators of oxidative stress in response to xenobiotics. The activity of superoxide dismutase was significantly increased in RAW cells, but not RBL cells exposed to the various Qdot treatments (Figure 17). The lack of oxidative stress in RBL cells may be due to the limited internalization of Qdots. A significant two-way interaction between size and concentration was observed in RAW cells (Table 8), with the 1 μM Qdot 520 treatment inducing the greatest response. The 1 μM Qdot 520-COOH, 1 nM and 1 μM Qdot 520-NH_2, and 1 nM Qdot 620-COOH treatments displayed significant increases in superoxide dismutase activity as compared with the control RAW cells (Table 9). Significant size-dependent differences in superoxide dismutase activity were also observed between the Qdot 520-COOH and Qdot 620-COOH, and Qdot 520-NH_2 and Qdot 620-NH_2 treatments (Table 9). The up-regulation of superoxide dismutase in response to Qdot may be linked to either free radical generation by the Qdots,[58] or release of Cd^{2+} from the Qdot core.[59] Interestingly, the oxidative stress response does not directly correlate with the observed toxicity induced by the Qdots. While considerable cell death in RAW cells occurred in the 1 μM Qdot 620 treatments (Figure 12A), only relatively smaller changes in the superoxide dismutase activity were observed for these treatments (Figure 17A). The significant increase in oxidative stress to the Qdot 520 treatments, however, suggests that further evaluation of intracellular effects (e.g., DNA damage) will be important for understanding the full toxicology and mechanisms of cell death related to Qdot exposure.

Table 8. Superoxide dismutase ANOVA statistics. P-vales from Three-way ANOVA test of single and multiple interaction effects of Qdot size, surface chemistry, and concentration on the levels of superoxide dismutase (SOD) in RAW macrophage cells and RBL mast cells. Values in bold text represent significant effects and interactions that are interpreted in the text.

	RAW	**RBL**
One-way effects		
Size	<0.001	0.806
Surface chemistry	0.628	0.418
Concentration	<0.001	0.323
Two-way effects		
Size x Surface chemistry	0.543	0.907
Size x Concentration	**<0.001**	0.749
Surface chemistry x Concentration	0.698	0.765
Three-way effects		
Size x Surface chemistry x Concentration	0.402	0.746

Table 9. Superoxide dismutase – treatment effects. ANOVA results for the comparison of the different Qdot treatments (i.e., size, surface chemistry, and concentration) on superoxide dismutase (SOD) levels in RAW and RBL cells exposed to QDots.

	RAW	RBL
Concentration		
520, COOH, nM vs. Control	No	No
520, NH_2, nM vs. Control	Yes	No
620, COOH, nM vs. Control	Yes	No
620, NH_2, nM vs. Control	No	No
520, COOH, µM vs. Control	Yes	No
520, NH_2, µM vs. Control	Yes	No
620, COOH, µM vs. Control	No	No
620, NH_2, µM vs. Control	No	No
520, COOH, µM vs. 520, COOH, nM	No	No
520, NH_2, µM vs. 520, NH_2, nM	No	No
620, COOH, µM vs. 620, COOH, nM	No	No
620, NH_2, µM vs. 620, NH_2, nM	No	No
Size		No
520, COOH, nM vs. 620, COOH, nM	No	No
520, COOH, µM vs. 620, COOH, µM	Yes	No
520, NH_2, nM vs. 620, NH_2, nM	No	No
520, NH_2, µM vs. 620, NH_2, µM	Yes	No
Surface chemistry		No
520, NH_2, nM vs. 520, COOH, nM	No	No
520, NH_2, µM vs. 520, COOH, µM	No	No
620, NH_2, nM vs. 620, COOH, nM	No	No
620, NH_2, µM vs. 620, COOH, µM	No	No

(A)

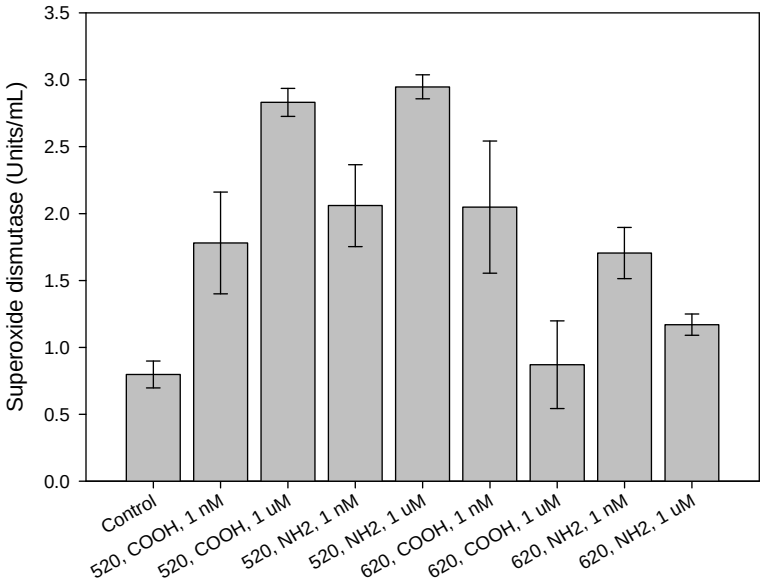

(B)

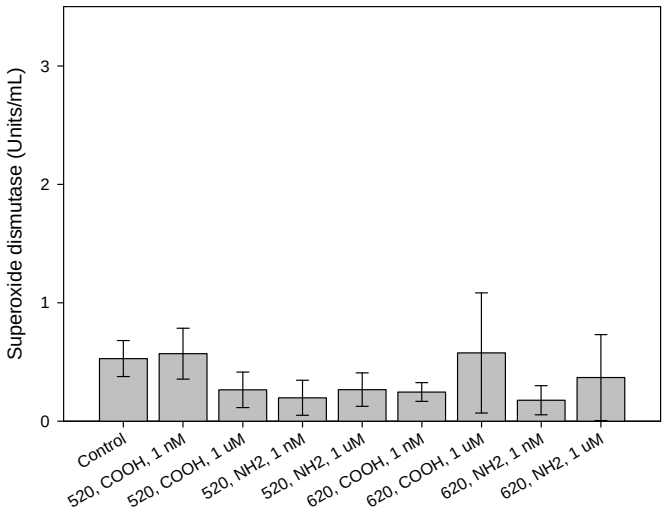

Figure 17. **RAW and RBL superoxide distmutase results.** Levels of superoxide dismutase activity in (**A**) RAW macrophage and (**B**) RBL mast cells measured at 18 hours after exposure to the different types of QDots. Error bars are the standard error of the mean.

4.0 Conclusions

The interaction, uptake, and biomolecular response of RAW macrophage and RBL mast cells were characterized as a function of the physical and chemical properties of Qdots. The basic experimental design followed a 2 x 2 x 3 factorial model in which the main effects and interactions among size (Qdot 520 and 620), surface chemistry (COOH and NH_2 surface groups), and concentration (0, 1 nM and 1 μM) were evaluated by Three-way Analysis of Variance (ANOVA). The uptake and biomolecular response to Qdot exposure in macrophage cells was primarily driven by a significant two-way interaction between Qdot size and concentration. Surface chemistry, in general, had minimal effects on uptake, toxicity, and response in RAW cells. Epifluorescence imaging demonstrated that cellular uptake was significantly greater for the larger Qdot 620 nanoparticles. Further, confocal imaging suggested that intracellular uptake of Qdots by macrophage cells occurred through an endocytotic pathway, and confirmed that internalization was dependent on Qdot size. A significant interaction between size and concentration was also observed with respect to Qdot-induced toxicity in RAW cells, with Qdot 620 nanoparticles inducing the greatest level of cell death. Analysis of cytokine release by macrophage cells demonstrated an increased in TNF-α, and decrease in IL-10 release in response to Qdot exposure that was dependent primarily on concentration and independent of size and surface chemistry. The co-varying changes in cytokine release suggested that the cells were experiencing a pro-inflammatory immune response to Qdot exposure. Lastly, RAW cells displayed increase activity of superoxide dismutase, an enzyme that helps protect cells against oxidative stress, which also was dependent on the interaction between Qdot size and concentration. The increased superoxide dismutase activity was observed in response to the smaller Qdot 520 nanoparticles, but not the Qdot 620 nanoparticles. Overall, these data demonstrate that Qdot size and concentration are the key factors that affect cellular uptake, toxicity, inflammatory response and oxidative stress in macrophage cells.

The association and biomolecular response of RBL mast cells were also driven by a two-way interaction between Qdot size and concentration, with minimal surface chemistry-dependent effects. Qdots displayed a primary interaction with RBL cell membranes and very limited uptake and intracellular distribution. A fundamental relationship between Qdot size and membrane association and distribution was also observed in RBL cells. Qdot 620 nanoparticles displayed a higher level of association and a more uniform distribution on the membrane surface as compared with the Qdot 520 nanoparticles. Quantitative fluorescence image analysis confirmed this dependency on the interaction of Qdot size and concentration. Despite minimal cellular uptake, a significant interaction between size and concentration was also observed with respect to Qdot-induced toxicity in RBL cells, with Qdot 620 nanoparticles inducing the greatest level of cell death. RBL toxicity is likely due to Qdot binding to membrane receptors and channels, or compromising the integrity of the cell membrane (e.g., through pore formation). This observation also indicates that Qdot-induced toxicity is independent of cellular uptake. In contrast to the increased cytokine release by RAW cells, RBL cells displayed a decrease in the release of TNF-α and IL-4 that was dependent on the interaction of Qdot size and concentration. This suppression in cytokine release is consistent with the hypothesis that membrane receptors and channels are being affected by Qdot binding. No change in the activity of superoxide dismutase was observed in RBL cells, suggesting that oxidative stress was not induced by Qdot interactions. Together these results demonstrate that Qdot exposure can trigger considerably different responses based on their interaction/uptake at the cell membrane surface.

Cell death and biomolecular response in both RBL and RAW cells were primarily observed at the high (i.e., 1 μM) concentrations of Qdots and with the larger Qdot 620 nanoparticles. Such dose-dependent effects to xenobiotics are common. It will be crucial to further investigate a wide range of Qdot concentrations to establish useful toxicological data (e.g., LD_{50} values) related to the environmental and health safety of these materials. Future evaluation of the size-dependency and size-concentration interaction is needed to fully understand how these relationships correlate with toxicology. Such an understanding will be crucial to developing predictive models of toxicity and risk of engineered nanoparticles to human and environmental health.

5.0 References

1. Smith, N.J., Emmett, K.J., and Rosenthal, S.J., Photovoltaic cells fabricated by electrophoretic deposition of CdSe nanocrystals. *Appl. Phys. Lett.* **93**, 3 (2008).
2. Leschkies, K.S., Divakar, R., Basu, J., Enache-Pommer, E., Boercker, J.E., Carter, C.B., Kortshagen, U.R., Norris, D.J., and Aydil, E.S., Photosensitization of ZnO nanowires with CdSe quantum dots for photovoltaic devices. *Nano Lett.* **7**, 1793 (2007).
3. McDonald, S.A., Konstantatos, G., Zhang, S.G., Cyr, P.W., Klem, E.J.D., Levina, L., and Sargent, E.H., Solution-processed PbS quantum dot infrared photodetectors and photovoltaics. *Nat. Mater.* **4**, 138 (2005).
4. Gobin, A.M., Lee, M.H., Halas, N.J., James, W.D., Drezek, R.A., and West, J.L., Near-infrared resonant nanoshells for combined optical imaging and photothermal cancer therapy. *Nano Lett.* **7**, 1929 (2007).
5. Loo, C., Hirsch, L., Lee, M.H., Chang, E., West, J., Halas, N., and Drezek, R., Gold nanoshell bioconjugates for molecular imaging in living cells. *Opt. Lett.* **30**, 1012 (2005).
6. Gao, X.H., Cui, Y.Y., Levenson, R.M., Chung, L.W.K., and Nie, S.M., In vivo cancer targeting and imaging with semiconductor quantum dots. *Nat. Biotechnol.* **22**, 969 (2004).
7. Pankhurst, Q.A., Connolly, J., Jones, S.K., and Dobson, J., Applications of magnetic nanoparticles in biomedicine. *J. Phys. D-Appl. Phys.* **36**, R167 (2003).
8. Akerman, M.E., Chan, W.C.W., Laakkonen, P., Bhatia, S.N., and Ruoslahti, E., Nanocrystal targeting in vivo. *Proc. Natl. Acad. Sci. U. S. A.* **99**, 12617 (2002).
9. Soppimath, K.S., Aminabhavi, T.M., Kulkarni, A.R., and Rudzinski, W.E., Biodegradable polymeric nanoparticles as drug delivery devices. *J. Control. Release* **70**, 1 (2001).
10. Kane, A.B. and Hurt, R.H., Nanotoxicology: The asbestos analogy revisited. *Nat. Nanotechnol.* **3**, 378 (2008).
11. Seetharam, R.N. and Sridhar, K.R., Nanotoxicity: Threat posed by nanoparticles. *Curr. Sci.* **93**, 769 (2007).
12. Mnyusiwalla, A., Daar, A.S., and Singer, P.A., 'Mind the gap': science and ethics in nanotechnology. *Nanotechnology* **14**, R9 (2003).
13. Schulte, P.A. and Salamanca-Buentello, F., Ethical and scientific issues of nanotechnology in the workplace. *Environ. Health Perspect.* **115**, 5 (2007).
14. Balbus, J.M., Florini, K., Denison, R.A., and Walsh, S.A., in *Living in a Chemical World: Framing the Future in Light of the Past* (Blackwell Publishing, Oxford, 2006), Vol. 1076, pp. 331.
15. Oberdorster, G., Concepts of nanotoxicology. *Environ. Mol. Mutagen.* **48**, 532 (2007).
16. Lewinski, N., Colvin, V., and Drezek, R., Cytotoxicity of nanoparticles. *Small* **4**, 26 (2008).
17. Kwon, J.T., Hwang, S.K., Jin, H., Kim, D.S., Mina-Tehrani, A., Yoon, H.J., Chop, M., Yoon, T.J., Han, D.Y., Kang, Y.W., Yoon, B.I., Lee, J.K., and Cho, M.H., Body distribution of inhaled fluorescent magnetic nanoparticles in the mice. *J. Occup. Health* **50**, 1 (2008).
18. Kim, J.S., Yoon, T.J., Kim, B.G., Park, S.J., Kim, H.W., Lee, K.H., Park, S.B., Lee, J.K., and Cho, M.H., Toxicity and tissue distribution of magnetic nanoparticles in mice. *Toxicol. Sci.* **89**, 338 (2006).
19. Poland, C.A., Duffin, R., Kinloch, I., Maynard, A., Wallace, W.A.H., Seaton, A., Stone, V., Brown, S., MacNee, W., and Donaldson, K., Carbon nanotubes introduced into the abdominal cavity of mice show asbestos-like pathogenicity in a pilot study. *Nat. Nanotechnol.* **3**, 423 (2008).
20. Garza, K.M., Soto, K.F., and Murr, L.E., Cytotoxicity and reactive oxygen species generation from aggregated carbon and carbonaceous nanoparticulate materials. *Int. J. Nanomed.* **3**, 83 (2008).
21. Lusk, J.L. and Rozan, A., Public policy and endogenous beliefs: The case of genetically modified food. *J. Agric. Resour. Econ.* **33**, 270 (2008).
22. Auer, C., Ecological risk assessment and regulation for genetically-modified ornamental plants. *Crit. Rev. Plant Sci.* **27**, 255 (2008).
23. Nap, J.P., Metz, P.L.J., Escaler, M., and Conner, A.J., The release of genetically modified crops into the environment - Part I. Overview of current status and regulations. *Plant J.* **33**, 1 (2003).
24. Conner, A.J., Glare, T.R., and Nap, J.P., The release of genetically modified crops into the environment - Part II. Overview of ecological risk assessment. *Plant J.* **33**, 19 (2003).
25. Kuiper, H.A., Kleter, G.A., Noteborn, H., and Kok, E.J., Assessment of the food safety issues related to genetically modified foods. *Plant J.* **27**, 503 (2001).
26. Siegrist, M., The influence of trust and perceptions of risks and benefits on the acceptance of gene technology. *Risk Anal.* **20**, 195 (2000).
27. Baughman, R.H., Zakhidov, A.A., and de Heer, W.A., Carbon nanotubes - the route toward applications. *Science* **297**, 787 (2002).

28. Liu, J., Rinzler, A.G., Dai, H.J., Hafner, J.H., Bradley, R.K., Boul, P.J., Lu, A., Iverson, T., Shelimov, K., Huffman, C.B., Rodriguez-Macias, F., Shon, Y.S., Lee, T.R., Colbert, D.T., and Smalley, R.E., Fullerene pipes. *Science* **280**, 1253 (1998).
29. Liu, J., Dai, H.J., Hafner, J.H., Colbert, D.T., Smalley, R.E., Tans, S.J., and Dekker, C., Fullerene 'crop circles'. *Nature* **385**, 780 (1997).
30. Thess, A., Lee, R., Nikolaev, P., Dai, H.J., Petit, P., Robert, J., Xu, C.H., Lee, Y.H., Kim, S.G., Rinzler, A.G., Colbert, D.T., Scuseria, G.E., Tomanek, D., Fischer, J.E., and Smalley, R.E., Crystalline ropes of metallic carbon nanotubes. *Science* **273**, 483 (1996).
31. Niemeyer, C.M., Nanoparticles, proteins, and nucleic acids: Biotechnology meets materials science. *Angew. Chem.-Int. Edit.* **40**, 4128 (2001).
32. Sun, S.H., Murray, C.B., Weller, D., Folks, L., and Moser, A., Monodisperse FePt nanoparticles and ferromagnetic FePt nanocrystal superlattices. *Science* **287**, 1989 (2000).
33. Kelly, K.L., Coronado, E., Zhao, L.L., and Schatz, G.C., The optical properties of metal nanoparticles: The influence of size, shape, and dielectric environment. *J. Phys. Chem. B* **107**, 668 (2003).
34. Sun, Y.G. and Xia, Y.N., Shape-controlled synthesis of gold and silver nanoparticles. *Science* **298**, 2176 (2002).
35. Shipway, A.N., Katz, E., and Willner, I., Nanoparticle arrays on surfaces for electronic, optical, and sensor applications. *ChemPhysChem* **1**, 18 (2000).
36. Medintz, I.L., Uyeda, H.T., Goldman, E.R., and Mattoussi, H., Quantum dot bioconjugates for imaging, labelling and sensing. *Nat. Mater.* **4**, 435 (2005).
37. Burda, C., Chen, X.B., Narayanan, R., and El-Sayed, M.A., Chemistry and properties of nanocrystals of different shapes. *Chem. Rev.* **105**, 1025 (2005).
38. Bruchez, M., Moronne, M., Gin, P., Weiss, S., and Alivisatos, A.P., Semiconductor nanocrystals as fluorescent biological labels. *Science* **281**, 2013 (1998).
39. Tian, Z.R.R., Voigt, J.A., Liu, J., McKenzie, B., McDermott, M.J., Rodriguez, M.A., Konishi, H., and Xu, H.F., Complex and oriented ZnO nanostructures. *Nat. Mater.* **2**, 821 (2003).
40. Tian, Z.R.R., Voigt, J.A., Liu, J., McKenzie, B., and McDermott, M.J., Biommetic arrays of oriented helical ZnO nanorods and columns. *J. Am. Chem. Soc.* **124**, 12954 (2002).
41. Chan, W.C.W., Maxwell, D.J., Gao, X.H., Bailey, R.E., Han, M.Y., and Nie, S.M., Luminescent quantum dots for multiplexed biological detection and imaging. *Curr. Opin. Biotechnol.* **13**, 40 (2002).
42. Alivisatos, A.P., Semiconductor clusters, nanocrystals, and quantum dots. *Science* **271**, 933 (1996).
43. Peng, X.G., Wickham, J., and Alivisatos, A.P., Kinetics of II-VI and III-V colloidal semiconductor nanocrystal growth: "Focusing" of size distributions. *J. Am. Chem. Soc.* **120**, 5343 (1998).
44. Domingo, J.L., Metal-Induced Developmental Toxicity in Mammals - a Review. *J. Toxicol. Environ. Health* **42**, 123 (1994).
45. Wang, Q., Kuo, Y.C., Wang, Y.W., Shin, G., Ruengruglikit, C., and Huang, Q.R., Luminescent properties of water-soluble denatured bovine serum albumin-coated CdTe quantum dots. *J. Phys. Chem. B* **110**, 16860 (2006).
46. Han, H.Y., Hu, D.H., Liang, J.G., and Sheng, Z.H., Study on the interaction between CdSe quantum dots and bovine serum albumin with ultraviolet visible absorption spectroscopy. *Chin. Chem. Lett.* **17**, 961 (2006).
47. Oh, M.H.J., Gentleman, D.J., and Scholes, G.D., Water soluble quantum dot nanoclusters: Energy migration in artificial materials. *Phys. Chem. Chem. Phys.* **8**, 5079 (2006).
48. Clift, M.J.D., Rothen-Rutishauser, B., Brown, D.M., Duffin, R., Donaldson, K., Proudfoot, L., Guy, K., and Stone, V., The impact of different nanoparticle surface chemistry and size on uptake and toxicity in a murine macrophage cell line. *Toxicol. Appl. Pharmacol.* **232**, 418 (2008).
49. Hoshino, A., Fujioka, K., Oku, T., Suga, M., Sasaki, Y.F., Ohta, T., Yasuhara, M., Suzuki, K., and Yamamoto, K., Physicochemical properties and cellular toxicity of nanocrystal quantum dots depend on their surface modification. *Nano Lett.* **4**, 2163 (2004).
50. Ryman-Rasmussen, J.P., Riviere, J.E., and Monteiro-Riviere, N.A., Surface coatings determine cytotoxicity and irritation potential of quantum dot nanoparticles in epidermal keratinocytes. *J. Invest. Dermatol.* **127**, 143 (2007).
51. Peng, X.G., Manna, L., Yang, W.D., Wickham, J., Scher, E., Kadavanich, A., and Alivisatos, A.P., Shape control of CdSe nanocrystals. *Nature* **404**, 59 (2000).
52. Pierini, L., Holowka, D., and Baird, B., Fc epsilon RI-mediated association of 6-mu m beads with RBL-2H3 mast cells results in exclusion of signaling proteins from the forming phagosome and abrogation of normal downstream signaling. *J. Cell Biol.* **134**, 1427 (1996).

53. Zhang, Y.B., Chen, W., Zhang, J., Liu, J., Chen, G.P., and Pope, C., In vitro and in vivo toxicity of CdTe nanoparticles. *J. Nanosci. Nanotechnol.* **7**, 497 (2007).
54. Shiohara, A., Hoshino, A., Hanaki, K., Suzuki, K., and Yamamoto, K., On the cyto-toxicity caused by quantum dots. *Microbiol. Immunol.* **48**, 669 (2004).
55. Ramachandran, S., Merrill, N.E., Blick, R.H., and Weide, D.W.v.d., Colloidal quantum dots initiating current bursts in lipid bilayers. *Biosens. Bioelectron.* **20**, 2173 (2005).
56. Manna, S.K., Sarkar, S., Barr, J., Wise, K., Barrera, E.V., Jejelowo, O., Rice-Ficht, A.C., and Ramesh, G.T., Single-walled carbon nanotube induces oxidative stress and activates nuclear transcription factor-kappa B in human keratinocytes. *Nano Lett.* **5**, 1676 (2005).
57. Cho, S.J., Maysinger, D., Jain, M., Roder, B., Hackbarth, S., and Winnik, F.M., Long-term exposure to CdTe quantum dots causes functional impairments in live cells. *Langmuir* **23**, 1974 (2007).
58. Ipe, B.I., Lehnig, M., and Niemeyer, C.M., On the generation of free radical species from quantum dots. *Small* **1**, 706 (2005).
59. Nzengue, Y., Steiman, R., Garrel, C., Lefebvre, E., and Guiraud, P., Oxidative stress and DNA damage induced by cadmium in the human keratinocyte HaCaT cell line: Role of glutathione in the resistance to cadmium. *Toxicology* **243**, 193 (2008).

Distribution (electronics copies)

1	MS 0123	Donna Chavez, LDRD Office	1011
1	MS 0899	Technical Library	9536
1	MS 0351	Richard Stulen	1000
1	MS 1413	Grant S. Heffelfinger	8630
1	MS 9054	Glenn D. Kubiak	8600
1	MS 6100	Terry Michalske	6100
1	MS 1315	Bob Hwang	1130
1	MS 1315	Neal Shinn	1131
1	MS 1427	Julia Phillips	1100
1	MS 1303	George D. Bachand	1132
1	MS 1303	Marlene Bachand	1132
1	MS 1303	Adrienne C. Greene	1132
1	MS 0895	Tony Martino	8332
1	MS 1413	Jens Poschet	8332
1	MS 1413	J. Bryce Ricken	8332
1	MS 0895	Jeri Timlin	8332
1	MS 1413	Jesse Aaron	8332
1	MS 1411	Bruce C. Bunker	1816
1	MS 0892	Susan Brozik	1714